C.P. No. 1261

C.P. No. 1261

MINISTRY OF DEFENCE (PROCUREMENT EXECUTIVE)

AERONAUTICAL RESEARCH COUNCIL

CURRENT PAPERS

NPL 9615 and NACA 0012
A Comparison of Aerodynamic Data

By

N. Gregory and P. G. Wilby

Aerodynamics Division, NPL

LONDON: HER MAJESTY'S STATIONERY OFFICE

1973

PRICE 80p NET

CP No. 1261*
November, 1968

NPL 9615 AND NACA 0012 - A COMPARISON OF AERODYNAMIC DATA

- by -

N. Gregory and P. G. Wilby

Aerodynamics Division, NPL

SUMMARY

Ordinates, surface slopes and curvatures are listed for the two aerofoils together with a detailed tabulation of lift, drag and pitching moment data obtained at Mach numbers between 0.3 and 0.85 in the NPL 36 in. × 14 in. transonic tunnel. The aerodynamic characteristics and all the pressure distribution are plotted, with some comparisons.

1. Introduction

NACA 0012 is a standard section frequently used for helicopter rotors and NPL 9615 is a derivative of it having a 6.2% extension to the chord and a drooped leading edge with larger radius of curvature. The position of NPL 9615 in the current programme of aerofoil section development for helicopter use will be reported on separately, but as this section has been found to possess advantages over NACA 0012, its description and measured aerodynamic characteristics are given herewith and some comparisons are drawn.

2. Section Shapes

The NACA four-digit series of wing sections was first reported on in 1932[1], and the following formulae for the thickness distribution and leading edge radius are taken from Ref. 2.

$$\pm y/c = \frac{t/c}{0.20}\left(0.29690\sqrt{x/c} - 0.12600\,x/c - 0.35160\,(x/c)^2 + 0.28430\,(x/c)^3 - 0.10150\,(x/c)^4\right)$$

$$R_o/c = 1.1019\,(t/c)^2$$

NACA 0012 is obtained by putting $t/c = 0.12$ in the above equations, and the ordinates are listed in TABLE 1 together with surface slopes and curvatures.

The new section, NPL 9615, was obtained by taking the rear portion NACA 0012 and modifying ordinates forward of the position of maximum thickness, extending and drooping the nose. The ordinates for NPL 9615 are non-dimensionalised with respect to the extended chord and are listed in TABLE 2, also with surface

slopes/

---

*Replaces A.R.C.30 657 - NPL Aero Special Report 017.

slopes and curvatures. The nose portions of the aerofoils are compared in Fig. 1 and the upper surface curvature distributions ahead of position of maximum thickness are compared in Fig. 2. The thickness/chord ratio of NPL 9615 is 0.113 compared with 0.12 of NACA 0012, and the new profile blends smoothly into the NACA 0012 rear portion at x/c (based on the new chord and nose position as origin) equal to 0.28333 for the upper surface and equal to 0.3409, the position for maximum thickness, on the lower.

The leading-edge radius of NPL 9615 is 0.01883, non-dimensionalised in terms of the actual chord. This should be compared with 0.0158 for the standard NACA 0012, (a figure which is reduced to 0.0141 for a NACA four-digit thickness distribution with the 11.3% thickness/chord ratio of NPL 9615).

One of the aims of the design features of NPL 9615 was to reduce the curvature of the upper surface, relative to that for NACA 0012, in the region where supersonic flow develops at incidence. This helps to reduce the maximum velocities and hence the strength of the shock wave that terminates the supersonic region. The reduction of curvature was made possible by the extended leading edge which also allowed the incorporation of leading-edge droop and an increase of leading-edge radius, both of which help to increase the low speed $C_{L_{max}}$. The droop and increased radius also have an effect on the development of the local supersonic flow.

3. Test Conditions

The aerodynamic data for the two sections were obtained under identical conditions so that the comparison should not be influenced by these conditions. The tests were carried out with 10 in. (0.254 m.) chord models spanning to 14 in. (0.356 m.) dimension of the NPL 36 in. × 14 in. (0.92 m. × 0.36 m.) transonic wind-tunnel, which operates at atmospheric stagnation pressure. The floor and ceiling of the tunnel were slotted (4 slots, overall open-area ratio = 0.33) and were 31 in. (0.79 m.) apart throughout the length of the working section. These conditions are close to those giving blockage-free and lift-interference-free results, and no corrections for wall constraint have been applied.

Further tests are now in hand to determine optimum test conditions and to calibrate the tunnel precisely. Lift interference and blockage are affected by both wall divergence and open-area ratio and it is not clear whether a wall configuration can be found to give zero values of lift interference and blockage simultaneously, or whether such a wall would remain entirely interference-free at the high values of C_L and Mach number which need to be covered in the present tests.

For the present, it should suffice that any neglected constraint corrections should be small, and may be equivalent to a small change in free-stream Mach number. Furthermore, the comparison between the two sections should not be influenced by whether the identical test conditions are entirely interference-free. In one respect they are not: the thick end-wall boundary layers lead to a serious departure from two-dimensional testing conditions at high angles of incidence and hence to a reduction in $C_{L_{max}}$.

Companion tests have been carried out in the 13 ft × 9 ft low speed wind tunnel on a model of NACA 0012. Although the end effects are much further removed from mid-span with a planform aspect ratio of 3.6 compared with 1.4 for the 36 in. × 14 in. wind tunnel, the tests revealed a gain in $C_{L\,max}$ of over 0.1 when premature flow separation at the ends was inhibited by boundary-layer control by suction.

All/

All results were obtained with a roughness band of 230-270 mesh carborundum* present between the leading edge and 0.02 chord on both surfaces. Sufficient roughness was required to produce boundary-layer transition ahead of strong shocks in order to avoid optimistic values for $C_{L\ max}$ at high Mach number. On the other hand, too much roughness was likely to produce low values of $C_{L\ max}$ at low speed and a high overall level of drag. The band that was chosen provided a compromise roughness that could be used over the whole range of the tests and gave a reasonable simulation of the conditions on a full-scale helicopter blade. However, the most important point to note is that the same roughness band was used on both models so as to ensure a valid comparison of one set of results with the other. Direct-shadow photographs revealed that with the band present, transition occurred between 0.10 and 0.40 chord downstream of the band, depending on Mach number and pressure gradient. Without the band, transition would have occurred in an unrealistic position much further aft.

4. Results

Lift and pitching moment were found by integration from the distribution of pressure round the centre portion of the aerofoil measured at about 43 static pressure hole stations in the surface of the model. Profile drag was obtained by wake traverse.

The measurements were taken in order to construct tables of aerodynamic characteristics at 0.05 intervals in Mach number and $\frac{1}{2}°$ intervals in incidence required as input for the comparative machine computation of rotor performance and it was therefore necessary to double-smooth the experimental observations. This has therefore already been done and the tables here presented contain the smoothed values, limited to the (M, α) regions actually covered by the tests, and obtained by interpolation where necessary: Only a few of the $\frac{1}{2}°$ settings were actually tested. The graphs on the other hand make use of values measured at 0.025 intervals in Mach number in regions where the values are varying rapidly. TABLE 3 lists values of C_L, C_D and $C_{m_{c/4}}$ for NPL 9615 at Mach numbers between 0.3 and 0.85 with incidences between $-2°$ and the stall, and TABLE 4 contains corresponding information at positive values of incidence for the symmetrical section NACA 0012. The test Reynolds number varied from 1.7×10^6 at $M = 0.3$ to 3.75×10^6 at $M = 0.85$. Curves showing the variation at C_L, C_D, and $C_{m_{c/4}}$ with incidence are plotted in Figs. 3, 4 and 5 for NPL 9615, and in Figs. 6, 7 and 8 for NACA 0012.

The pressure distributions for NPL 9615 are plotted for each incidence in Figs. 9 a - q. Up to 3° incidence the upper and lower surface distributions are plotted separately; above this incidence the two distributions are combined on the same diagram. Corresponding pressure distributions for NACA 0012 are shown in Figs. 10 a - m, for positive incidences up to 12°.

5. Some Comparisons

The effect of the profile changes referred to in Section 2 on the aerodynamic characteristics of the two sections is summarised in Fig. 11. This figure shows an improvement in the values of $C_{L\ max}$ over the whole Mach number range of the tests and also gives boundaries in the (M, C_L) plane for the onset of a rapid change in pitching moment and for the onset of a rapid rise in drag. The latter boundaries are not easily defined everywhere, and are only approximate in their location. In particular, at incidences below 1°, NPL 9615 exhibits a pronounced drag creep preceding the more rapid rise, as can be seen at zero lift in the drag comparison of Fig. 12. This figure serves to emphasize another limitation of Fig. 11. This is that the values of C_D, C_m and α differ

in/

*230-270 mesh carborundum implies grains that were sieved through a gauge with 230 wires to the linear inch, but which were retained by a gauge with 270 wires to the inch. This implies grains that passed through a square aperture with side 0.0027 in. (0.062 mm) but not through one with side 0.0023 in. (0.053 mm).

in general between the two sections at any point on that figure, and also along the boundaries: the values must be inferred from the Tables, but are shown in some more detailed comparisons which follow.

NPL 9615 has slightly larger zero-lift drag than NACA 0012 at Mach numbers below drag rise, (Fig. 12), though its critical Mach number for rapid drag rise is marginally greater, and beyond this point its rate of increase of drag is appreciably less. This latter feature occurs also at non-zero values of C_L, both with respect to increase of Mach number and also with respect to increases of C_L at constant Mach number, as can be seen from the comparison of drag polars, Fig. 13.

Drag reductions are obtained in regions of high drag at all Mach numbers, with both sub-critical and super-critical flow. The largest drag reductions are obtained at Mach numbers between 0.55 and 0.65, a range that covers the tip Mach numbers of many helicopter rotors, and at values of C_L in the region of $C_{L\ max}$ for NACA 0012, the saving in drag can amount to as much as 30%. In super-critical flow, a comparison of typical pressure distributions is made in Fig. 14 for a Mach number of 0.6 and a C_L value of 0.76. (The distribution for NPL 9615 was interpolated between two observations). It will be seen that the profile change has reduced the velocities in the supersonic region as expected, and this has resulted in the desired reduction in shock strength, and hence in wave drag.

The improvements in $C_{L\ max}$ and the reductions in the high-drag level together result in an improvement in the maximum value of the lift/drag ratio over the whole Mach number range of the comparison, Fig. 15.

The pitching-moment variations with Mach number are compared in Fig. 16 for angles of 3° and below. On account of its camber, NPL generally shows a nose-down bias compared with that for the symmetrical section: this also shows up at zero-lift, Fig. 17. At high Mach numbers, the pitching moments on both sections change rapidly.

6. Conclusions

A slightly drooped extension with larger radii of curvature at the leading edge and on the upper surface has been fitted to NACA 0012. This reduces the maximum velocities in the supersonic region at high Mach numbers and also the strength of the shock wave that terminates it.

The modification has reduced the thickness/chord ratio from 12% to 11.3%, but a zero-lift pitching-moment coefficient at M = 0.3 of -0.008 has arisen because of the droop (Fig. 17). The following benefits have been secured by the re-design:-

An increase in $C_{L\ max}$ of between 0.08 and 0.14 at Mach numbers below 0.65 (Fig. 15) despite the reduction in thickness/chord ratio.

An increase of about 0.02 in the drag-rise Mach number (Figs. 15, 18).

A reduction of drag in the high-drag region, particularly where supersonic flow is present. At values of C_L in the region of $C_{L\ max}$ for NACA 0012, the saving in drag can amount to as much as 30% (Fig. 13).

The maximum values of lift/drag ratio are increased at all Mach numbers (Fig. 14).

Conclusions/

Acknowledgement

The work herein reported was carried out as a team effort. Particular acknowledgement must be made of the parts played by Mr. V. G. Quincey in charge of the 36 in. x 14.in. wind tunnel and by Miss E. M. Love in preparing the smoothed data and the Figures.

References

No.	Author(s)	Title, etc.
1	Eastman N. Jacobs K. E. Ward and R. M. Pinkerton	The characteristics of 78 related sections from tests in the variable-density wind tunnel. NACA Rpt. 460, 1932.
2	I. R. Abbott and A. E. van Doenhoff	Theory of wing sections. McGrew Hill, 1949.

TABLE I/

TABLE I

NACA 0012 ORDINATES

$\frac{x}{c}$	$\frac{y}{c}$	θ	ρ
0	0	90	63.291
0.0005	0.0040	75.6	
0.0010	0.0056	70	
0.0025	0.0087	59.6	
0.0050	0.0122	49.8	
0.0075	0.0149	43.5	
0.0100	0.0170	39	21.062
0.0125	0.0189	35.6	
0.015	0.0206	32.8	
0.02	0.0236	28.6	10.893
0.03	0.0284	23.1	6.976
0.04	0.0323	19.5	4.985
0.05	0.0355	16.9	3.815
0.06	0.0383	14.8	
0.08	0.0430	11.8	
0.10	0.0469	9.6	1.663
0.12	0.0499	7.9	
0.14	0.0524	6.4	
0.16	0.0544	5.2	
0.18	0.0560	4.2	
0.20	0.0574	3.3	0.741
0.225	0.0586	2.3	0.644
0.25	0.0594	1.4	0.568
0.275	0.0599	0.7	0.505
0.3	0.0600	0	0.452
0.325	0.0599	-0.6	0.407
0.35	0.0595	-1.17	0.368
0.375	0.0588	-1.68	
0.4	0.0580	-2.13	0.305
0.425	0.0569	-2.55	
0.45	0.0558	-2.93	
0.475	0.0544	-3.29	
0.5	0.0529	-3.61	0.218
0.55	0.0495	-4.19	
0.6	0.0456	-4.70	0.165
0.65	0.0413	-5.14	
0.7	0.0366	-5.56	0.138
0.75	0.0315	-5.94	
0.8	0.0262	-6.32	0.131
0.85	0.0205	-6.70	
0.9	0.0145	-7.10	0.142
0.95	0.0080	-7.53	
1.00	0.0013	-8.02	0.169

θ = Surface slope, degrees

ρ = Surface curvature = c/R

Leading edge radius: $R_o/c = 1/\rho_o = 0.0158$

TABLE 2/

TABLE 2

NPI 9615 ORDINATES

θ	ρ	x/c	y/c
90	53.1	0	-0.01366
50	53.1	0.00443	-0.00155
45	32.5	0.00586	+0.00001
40	18	0.00857	0.00268
35	11	0.01359	0.00649
32.5	9	0.01726	0.00893
30	7.8	0.02172	0.01163
28	6.9	0.02589	0.01392
26	6.2	0.03065	0.01633
24	5.6	0.03602	0.01883
22	5.0	0.04209	0.02140
20	4.4	0.04905	0.02407
19	4.03	0.05297	0.02545
18	3.76	0.05723	0.02687
17	3.49	0.06183	0.02832
16	3.22	0.06682	0.02980
15	2.95	0.07227	0.03131
14	2.68	0.07828	0.03306
13.5	2.545	0.08152	0.03365
13	2.41	0.08495	0.03476
12.5	2.275	0.08858	0.03528
12	2.14	0.09244	0.03612
11.5	2.005	0.09656	0.03698
11	1.87	0.10098	0.03786
10.5	1.735	0.10574	0.03876
10	1.60	0.11076	0.03969
9.5	1.479	0.11622	0.04065
9	1.319	0.12239	0.04165
8.5	1.190	0.12928	0.04271
8	1.085	0.13688	0.04381
7.5	0.996	0.14520	0.04494
7	0.922	0.15403	0.04609
6.5	0.857	0.16378	0.04724
6	0.801	0.17425	0.04838
5.5	0.752	0.18544	0.04950
5	0.709	0.19734	0.05059
4.5	0.670	0.20995	0.05164
4	0.637	0.22358	0.05264
3.5	|	0.23700	0.05339
3	|	0.25094	0.05424
2.5	|	0.26450	0.05499
1.82	0.637	0.28333	0.05565
0.66		0.3175	0.0564
0		0.3409	0.0565
-0.618		0.3642	0.0564
-1.680		0.4115	0.0554
-2.133		0.4351	0.0546
-2.931		0.4821	0.0525
-3.611		0.5292	0.0498
-4.192		0.5763	0.0466
-4.696		0.6234	0.0430
-5.143		0.6704	0.0389
-5.557		0.7176	0.0345
-5.943		0.7646	0.0297
-6.320		0.8117	0.0247
-6.702		0.8588	0.0193
-7.098		0.9059	0.0136
-7.525		0.9529	0.0076
-7.750		0.9765	0.0045
-8.020		1.0000	0.0013
	LOWER SURFACE		
-90		0	-0.01366
-80.5		0.0002	-0.01600
-71		0.0008	-0.01810
-63.5		0.0019	-0.02080
-51		0.0033	-0.02300
-41.5		0.0056	-0.02540
-33.5		0.0089	-0.02780
-27		0.0130	-0.03010
-20.5		0.0184	-0.03245
-15.5		0.0236	-0.03415
-11		0.0290	-0.03540
- 9	2.5	0.03535	-0.03652
- 8.5	2.0	0.03884	
- 8	1.6	0.04330	-0.03781
- 7.5	1.15	0.04985	-0.03870
- 7	0.80	0.05900	-0.03986
- 6.5	0.55	0.07232	-0.04143
- 6	0.43	0.09030	-0.04340
- 5.75	0.417	0.10055	-0.04446
- 5.5	|	0.11098	-0.04547
- 5	|	0.13182	-0.04736
- 4.5	|	0.15269	-0.04911
- 4	|	0.17355	-0.05065
- 3.5	|	0.19444	-0.05202
- 3	|	0.21532	-0.05321
- 2.5	|	0.23624	-0.05422
- 2	|	0.25715	-0.05504
- 1.5	|	0.27806	-0.05568
- 1	|	0.29899	-0.05615
- 0.5	|	0.31990	-0.05640
0	0.417	0.34090	-0.05650

then as upper surface, with θ + ve, $\frac{y}{c}$ - ve.

$t/c = 0.113$

Leading edge radius: $Ro/c = 1/\rho_0 = 0.01883$, with centre at $x/c = 0.01883$, $y/c = -0.0137$

Profile is circular for 10° of arc on upper surface

Profile joins smoothly with NACA 0012 shape at $x/c = 0.28333$ on the upper surface and at $x/c = 0.3409$ on the lower surface

TABLE 3

NPL 9615

M	0.30			0.35			0.40		
α°	C_L	C_D	C_m	C_L	C_D	C_m	C_L	C_D	C_m
-2	-0.236	0.0096	-0.0111	-0.243	0.0099	-0.0081	-0.250	0.0102	-0.0076
-1½	-0.185	0.0096	-0.0098	-0.191	0.0099	-0.0080	-0.197	0.0101	-0.0079
-1	-0.134	0.0097	-0.0090	-0.139	0.0099	-0.0080	-0.143	0.0101	-0.0081
-½	-0.083	0.0099	-0.0085	-0.087	0.0100	-0.0081	-0.090	0.0102	-0.0083
0	-0.032	0.0101	-0.0081	-0.035	0.0102	-0.0082	-0.037	0.0103	-0.0084
½	0.019	0.0104	-0.0078	0.018	0.0103	-0.0082	0.017	0.0103	-0.0084
1	0.070	0.0106	-0.0075	0.071	0.0104	-0.0080	0.071	0.0103	-0.0084
1½	0.121	0.0107	-0.0075	0.123	0.0104	-0.0080	0.125	0.0102	-0.0083
2	0.172	0.0107	-0.0075	0.175	0.0103	-0.0080	0.179	0.0102	-0.0083
2½	0.223	0.0107	-0.0075	0.228	0.0104	-0.0080	0.233	0.0102	-0.0082
3	0.274	0.0106	-0.0076	0.281	0.0104	-0.0081	0.288	0.0103	-0.0082
3½	0.326	0.0105	-0.0077	0.334	0.0105	-0.0081	0.342	0.0105	-0.0082
4	0.377	0.0105	-0.0078	0.387	0.0105	-0.0081	0.397	0.0106	-0.0082
4½	0.429	0.0104	-0.0079	0.440	0.0106	-0.0081	0.451	0.0108	-0.0081
5	0.480	0.0103	-0.0078	0.493	0.0106	-0.0081	0.506	0.0110	-0.0081
5½	0.531	0.0100	-0.0061	0.546	0.0105	-0.0080	0.561	0.0112	-0.0081
6	0.583	0.0098	-0.0048	0.599	0.0102	-0.0078	0.615	0.0113	-0.0081
6½	0.635	0.0096	-0.0054	0.652	0.0101	-0.0066	0.670	0.0109	-0.0070
7	0.687	0.0097	-0.0070	0.706	0.0100	-0.0048	0.725	0.0105	-0.0045
7½	0.738	0.0100	-0.0078	0.759	0.0102	-0.0048	0.780	0.0107	-0.0040
8	0.790	0.0105	-0.0077	0.812	0.0106	-0.0051	0.834	0.0112	-0.0041
8½	0.841	0.0115	-0.0064	0.864	0.0116	-0.0052	0.888	0.0119	-0.0046
9	0.891	0.0127	-0.0051	0.915	0.0128	-0.0046	0.940	0.0129	-0.0039
9½	0.939	0.0140	-0.0037	0.963	0.0143	-0.0031	0.988	0.0145	-0.0018
10	0.986	0.0154	-0.0021	1.009	0.0157	-0.0014	1.032	0.0161	0.0006
10½	1.031	0.0168	-0.0006	1.053	0.0172	0.0006	1.073	0.0179	0.0034
11	1.074	0.0183	0.0010	1.096	0.0187	0.0027	1.113	0.0199	0.0064
11½	1.114	0.0199	0.0027	1.134	0.0207	0.0050	1.139	0.0224	0.0096
12	1.149	0.0219	0.0046	1.166	0.0232	0.0076	1.154	0.0261	0.0129
12½	1.180	0.0244	0.0068	1.191	0.0262	0.0102	1.162		
13	1.207	0.0273	0.0095	1.205	0.0298	0.0112			
13½	1.223	0.0307	0.0094						
14									

TABLE 3 (Contd)/

TABLE 3 (CONTD)

NPL 9615

M	0.45			0.50			0.55		
α°	C_L	C_D	C_m	C_L	C_D	C_m	C_L	C_D	C_m
-2	-0.257	0.0106	-0.0080	-0.264	0.0109	-0.0086	-0.271	0.0112	-0.0097
-1½	-0.202	0.0104	-0.0082	-0.208	0.0106	-0.0088	-0.213	0.0108	-0.0096
-1	-0.147	0.0103	-0.0085	-0.151	0.0105	-0.0089	-0.155	0.0105	-0.0095
-½	-0.092	0.0103	-0.0087	-0.094	0.0104	-0.0090	-0.096	0.0105	-0.0094
0	-0.037	0.0103	-0.0088	-0.037	0.0104	-0.0090	-0.038	0.0105	-0.0094
½	0.018	0.0103	-0.0087	0.019	0.0103	-0.0090	0.021	0.0104	-0.0094
1	0.073	0.0102	-0.0087	0.076	0.0103	-0.0090	0.080	0.0103	-0.0093
1½	0.129	0.0102	-0.0086	0.133	0.0103	-0.0088	0.139	0.0103	-0.0091
2	0.184	0.0102	-0.0085	0.190	0.0103	-0.0087	0.198	0.0103	-0.0089
2½	0.240	0.0102	-0.0084	0.247	0.0102	-0.0086	0.258	0.0103	-0.0087
3	0.296	0.0103	-0.0083	0.304	0.0103	-0.0085	0.317	0.0103	-0.0085
3½	0.351	0.0105	-0.0083	0.361	0.0105	-0.0083	0.376	0.0105	-0.0083
4	0.407	0.0106	-0.0082	0.419	0.0107	-0.0081	0.436	0.0107	-0.0080
4½	0.463	0.0108	-0.0080	0.476	0.0108	-0.0078	0.496	0.0109	-0.0076
5	0.520	0.0110	-0.0078	0.534	0.0110	-0.0075	0.557	0.0111	-0.0071
5½	0.576	0.0113	-0.0077	0.592	0.0113	-0.0071	0.619	0.0115	-0.0064
6	0.632	0.0116	-0.0075	0.650	0.0117	-0.0064	0.682	0.0119	-0.0054
6½	0.689	0.0120	-0.0062	0.708	0.0121	-0.0054	0.744	0.0124	-0.0040
7	0.745	0.0122	-0.0047	0.767	0.0126	-0.0044	0.805	0.0130	-0.0021
7½	0.801	0.0123	-0.0039	0.825	0.0130	-0.0033	0.865	0.0140	0.0003
8	0.857	0.0123	-0.0037	0.883	0.0134	-0.0014	0.924	0.0163	0.0034
8½	0.912	0.0126	-0.0026	0.941	0.0140	0.0016	0.982	0.0201	0.0070
9	0.965	0.0133	-0.0007	0.999	0.0150	0.0049	1.038	0.0241	0.0110
9½	1.013	0.0147	0.0022	1.046	0.0169	0.0083	1.068		0.0143
10	1.055	0.0169	0.0055	1.079	0.0203	0.0116	1.078		0.0157
10½	1.089	0.0194	0.0093	1.098	0.0245	0.0159			
11	1.116	0.0225	0.0130	1.105	0.0310	0.0186			
11½	1.132		0.0168						
12	1.132		0.0158						
12½									
13									
13½									
14									

TABLE 3 (Contd)/

TABLE 3 (CONTD)

NPL 9615

M	0.60			0.65			0.70		
α°	C_L	C_D	C_m	C_L	C_D	C_m	C_L	C_D	C_m
-2	-0.279	0.0115	-0.0116	-0.290	0.0123	-0.0142	-0.320	0.0153	-0.0179
$-1\frac{1}{2}$	-0.220	0.0110	-0.0106	-0.228	0.0118	-0.0118	-0.241	0.0129	-0.0133
-1	-0.160	0.0106	-0.0102	-0.165	0.0112	-0.0110	-0.170	0.0118	-0.0120
$-\frac{1}{2}$	-0.099	0.0105	-0.0100	-0.101	0.0107	-0.0106	-0.103	0.0112	-0.0115
0	-0.038	0.0105	-0.0098	-0.037	0.0106	-0.0103	-0.036	0.0108	-0.0110
$\frac{1}{2}$	0.023	0.0104	-0.0097	0.026	0.0105	-0.0100	0.030	0.0106	-0.0106
1	0.084	0.0103	-0.0095	0.089	0.0104	-0.0097	0.096	0.0104	-0.0102
$1\frac{1}{2}$	0.145	0.0103	-0.0093	0.153	0.0104	-0.0095	0.164	0.0104	-0.0099
2	0.207	0.0103	-0.0091	0.217	0.0104	-0.0093	0.235	0.0105	-0.0094
$2\frac{1}{2}$	0.270	0.0103	-0.0088	0.284	0.0104	-0.0089	0.308	0.0106	-0.0089
3	0.332	0.0103	-0.0086	0.351	0.0104	-0.0085	0.385	0.0108	-0.0082
$3\frac{1}{2}$	0.394	0.0105	-0.0083	0.419	0.0105	-0.0079	0.465	0.0120	-0.0076
4	0.456	0.0108	-0.0080	0.488	0.0110	-0.0067	0.546	0.0169	-0.0079
$4\frac{1}{2}$	0.520	0.0110	-0.0075	0.559	0.0117	-0.0051	0.623	0.0240	-0.0096
5	0.585	0.0113	-0.0066	0.633	0.0134	-0.0034	0.691	0.0320	-0.0133
$5\frac{1}{2}$	0.652	0.0118	-0.0051	0.712	0.0169	-0.0023	0.716		-0.0177
6	0.721	0.0126	-0.0031	0.794	0.0227	-0.0017	0.719		-0.0219
$6\frac{1}{2}$	0.792	0.0146	-0.0004	0.849		-0.0016			
7	0.861	0.0184	0.0027	0.876		-0.0025			
$7\frac{1}{2}$	0.927	0.0244	0.0055	0.890					
8	0.987	0.0307	0.0072						
$8\frac{1}{2}$	1.010								
9									
$9\frac{1}{2}$									
10									
$10\frac{1}{2}$									
11									
$11\frac{1}{2}$									
12									
$12\frac{1}{2}$									
13									
$13\frac{1}{2}$									
14									

TABLE 3 (Contd)/

TABLE 3 (CONCL)

NPL 9615

M	0.75			0.80			0.85		
α°	C_L	C_D	C_m	C_L	C_D	C_m	C_L	C_D	C_m
-2	-0.392	0.0166	-0.0208	-0.375	0.0364	-0.0036	-0.129		-0.0754
$-1\frac{1}{2}$	-0.298	0.0137	-0.0199	-0.317	0.0154	-0.0070	-0.100		-0.0692
-1	-0.207	0.0123	-0.0171	-0.241	0.0140	-0.0124	-0.083		-0.0553
$-\frac{1}{2}$	-0.117	0.0118	-0.0133	-0.145	0.0140	-0.0160	-0.071		-0.0334
0	-0.035	0.0113	-0.0118	-0.019	0.0148	-0.0194	-0.063		-0.0114
$\frac{1}{2}$	0.042	0.0111	-0.0112	0.082	0.0165	-0.0234	-0.058		+0.0102
1	0.118	0.0110	-0.0111	0.163	0.0190	-0.0281	-0.055		0.0316
$1\frac{1}{2}$	0.195	0.0114	-0.0113	0.228	0.0234	-0.0337			
2	0.273	0.0128	-0.0119	0.274	0.0317	-0.0366			
$2\frac{1}{2}$	0.356	0.0169	-0.0136	0.297		-0.0354			
3	0.448	0.0241	-0.0216	0.308		-0.0306			
$3\frac{1}{2}$	0.494		-0.0270						
4	0.517		-0.0293						
$4\frac{1}{2}$	0.520		-0.0302						
5	0.521		-0.0296						
$5\frac{1}{2}$									
6									
$6\frac{1}{2}$									
7									
$7\frac{1}{2}$									
8									
$8\frac{1}{2}$									
9									
$9\frac{1}{2}$									
10									
$10\frac{1}{2}$									
11									
$11\frac{1}{2}$									
12									
$12\frac{1}{2}$									
13									
$13\frac{1}{2}$									
14									

TABLE 4/

TABLE 4

NACA 0012

M	0.30			0.35			0.40		
$\alpha°$	C_L	C_D	C_m	C_L	C_D	C_m	C_L	C_D	C_m
-2									
-1½									
-1									
-½									
0	0.0	0.0103	0.0004	0.0	0.0103	0.0005	0.0	0.0103	0.0006
½	0.050	0.0103	0.0004	0.051	0.0103	0.0005	0.053	0.0103	0.0006
1	0.101	0.0103	0.0004	0.103	0.0103	0.0005	0.106	0.0103	0.0007
1½	0.152	0.0103	0.0005	0.158	0.0103	0.0006	0.160	0.0103	0.0008
2	0.204	0.0104	0.0007	0.208	0.0104	0.0007	0.213	0.0104	0.0009
2½	0.255	0.0104	0.0009	0.260	0.0104	0.0010	0.266	0.0104	0.0012
3	0.306	0.0106	0.0012	0.312	0.0106	0.0013	0.320	0.0106	0.0014
3½	0.358	0.0107	0.0015	0.366	0.0107	0.0016	0.375	0.0108	0.0017
4	0.409	0.0109	0.0019	0.419	0.0109	0.0020	0.430	0.0110	0.0021
4½	0.460	0.0110	0.0025	0.472	0.0111	0.0026	0.486	0.0112	0.0028
5	0.508	0.0111	0.0033	0.523	0.0113	0.0034	0.538	0.0115	0.0035
5½	0.555	0.0111	0.0041	0.568	0.0114	0.0042	0.585	0.0116	0.0045
6	0.602	0.0111	0.0048	0.616	0.0114	0.0050	0.630	0.0117	0.0056
6½	0.656	0.0112	0.0056	0.667	0.0114	0.0059	0.684	0.0117	0.0066
7	0.709	0.0114	0.0063	0.722	0.0116	0.0067	0.740	0.0118	0.0076
7½	0.765	0.0122	0.0070	0.777	0.0124	0.0075	0.796	0.0126	0.0087
8	0.819	0.0133	0.0077	0.834	0.0135	0.0084	0.852	0.0138	0.0098
8½	0.874	0.0147	0.0085	0.888	0.0150	0.0092	0.904	0.0153	0.0109
9	0.928	0.0162	0.0091	0.940	0.0165	0.0099	0.955	0.0170	0.0123
9½	0.979	0.0177	0.0099	0.988	0.0181	0.0112	0.998	0.0191	0.0138
10	1.020	0.0193	0.0107	1.024	0.0200	0.0126	1.033	0.0218	0.0159
10½	1.056	0.0212	0.0116	1.056		0.0146	1.060		0.0185
11	1.090	0.0233	0.0125	1.087		0.0169	1.080		0.0204
11½	1.120	0.0259	0.0135	1.106					
12	1.144	0.0294	0.0149	1.000					
12½									
13									
13½									
14									

TABLE 4 (Contd)/

TABLE 4 (CONTD)

NACA 0012

M	0.45			0.50			0.55		
α°	C_L	C_D	C_m	C_L	C_D	C_m	C_L	C_D	C_m
-2									
-1½									
-1									
-½									
0	0.0	0.0102	0.0007	0.0	0.0101	0.0008	0.0	0.0100	0.0009
½	0.054	0.0102	0.0007	0.056	0.0101	0.0009	0.058	0.0100	0.0011
1	0.108	0.0102	0.0009	0.112	0.0101	0.0011	0.116	0.0101	0.0014
1½	0.164	0.0102	0.0010	0.167	0.0102	0.0013	0.174	0.0102	0.0017
2	0.218	0.0103	0.0012	0.225	0.0102	0.0016	0.234	0.0103	0.0021
2½	0.273	0.0104	0.0014	0.283	0.0104	0.0019	0.295	0.0105	0.0026
3	0.330	0.0107	0.0017	0.342	0.0107	0.0022	0.356	0.0107	0.0030
3½	0.387	0.0109	0.0019	0.399	0.0110	0.0026	0.416	0.0110	0.0035
4	0.443	0.0111	0.0024	0.458	0.0113	0.0030	0.478	0.0113	0.0045
4½	0.500	0.0114	0.0030	0.518	0.0116	0.0037	0.540	0.0117	0.0054
5	0.557	0.0116	0.0039	0.578	0.0120	0.0045	0.602	0.0123	0.0068
5½	0.604	0.0118	0.0050	0.631	0.0124	0.0059	0.662	0.0130	0.0090
6	0.652	0.0120	0.0063	0.684	0.0128	0.0077	0.723	0.0139	0.0114
6½	0.706	0.0122	0.0077	0.736	0.0132	0.0098	0.783	0.0154	0.0141
7	0.761	0.0124	0.0092	0.790	0.0139	0.0119	0.840	0.0174	0.0169
7½	0.816	0.0133	0.0106	0.848	0.0151	0.0142	0.891	0.0205	0.0200
8	0.871	0.0146	0.0120	0.899	0.0174	0.0167	0.938	0.0260	0.0225
8½	0.924	0.0166	0.0139	0.943	0.0216	0.0197	0.900	0.0384	0.0164
9	0.973	0.0192	0.0162	0.967	0.0300	0.0232	0.844		-0.0022
9½	1.004		0.0190	0.935		0.0111			
10	1.013		0.0228	0.845		-0.0134			
10½									
11									
11½									
12									
12½									
13									
13½									
14									

TABLE 4 (Contd)/

TABLE 4 (CONTD)

NACA 0012

M	0.60			0.65			0.70		
$\alpha°$	C_L	C_D	C_m	C_L	C_D	C_m	C_L	C_D	C_m
-2									
-1½									
-1									
-½									
0	0.0	0.0100	0.0010	0.0	0.0100	0.0011	0.0	0.0101	0.0012
½	0.060	0.0100	0.0013	0.063	0.0101	0.0016	0.068	0.0102	0.0019
1	0.120	0.0101	0.0017	0.128	0.0102	0.0021	0.138	0.0103	0.0025
1½	0.182	0.0102	0.0022	0.193	0.0103	0.0027	0.213	0.0104	0.0034
2	0.245	0.0103	0.0028	0.260	0.0104	0.0036	0.288	0.0106	0.0044
2½	0.309	0.0106	0.0034	0.328	0.0107	0.0046	0.366	0.0114	0.0055
3	0.373	0.0108	0.0041	0.397	0.0111	0.0058	0.442	0.0135	0.0068
3½	0.439	0.0110	0.0052	0.470	0.0116	0.0072	0.517	0.0175	0.0075
4	0.504	0.0114	0.0064	0.542	0.0123	0.0085	0.593	0.0245	0.0068
4½	0.569	0.0119	0.0081	0.616	0.0151	0.0099	0.648		0.0041
5	0.634	0.0127	0.0104	0.691	0.0209	0.0116	0.672		0.0004
5½	0.700	0.0150	0.0131	0.752	0.0275	0.0135	0.667		-0.0046
6	0.764	0.0184	0.0158	0.796	0.0356	0.0146	0.657		-0.0095
6½	0.826	0.0230	0.0190	0.805	0.0475	0.0102			
7	0.882	0.0293	0.0217	0.780	0.0679	0.0014			
7½	0.876	0.0391	0.0178						
8	0.836		0.0048						
8½									
9									
9½									
10									
10½									
11									
11½									
12									
12½									
13									
13½									
14									

TABLE 4 (Contd)/

TABLE 4 (CONCL)

NACA 0012

M	0.75			0.80			0.85		
α°	C_L	C_D	C_m	C_L	C_D	C_m	C_L	C_D	C_m
-2									
-1½									
-1									
-½									
0	0.001	0.0104	0.0015	0.005	0.0176	0.0018	0.013		-0.0009
½	0.080	0.0107	0.0024	0. 00	0.0200	-0.0054	0.020		+0.014
1	0.160	0.0110	0.0031	0.201	0.0265	-0.0120	0.020		0.040
1½	0.244	0.0118	0.0022	0.265	0.0370	-0.0169			
2	0.328	0 0170	-0.0004	0.275		-0.0208			
2½	0.408		-0.0037						
3	0.482		-0.0078						
3½	0.500		-0.0121						
4	0.500		-0.0166						
4½									
5									
5½									
6									
6½									
7									
7½									
8									
8½									
9									
9½									
10									
10½									
11									
11½									
12									
12½									
13									
13½									
14									

EM

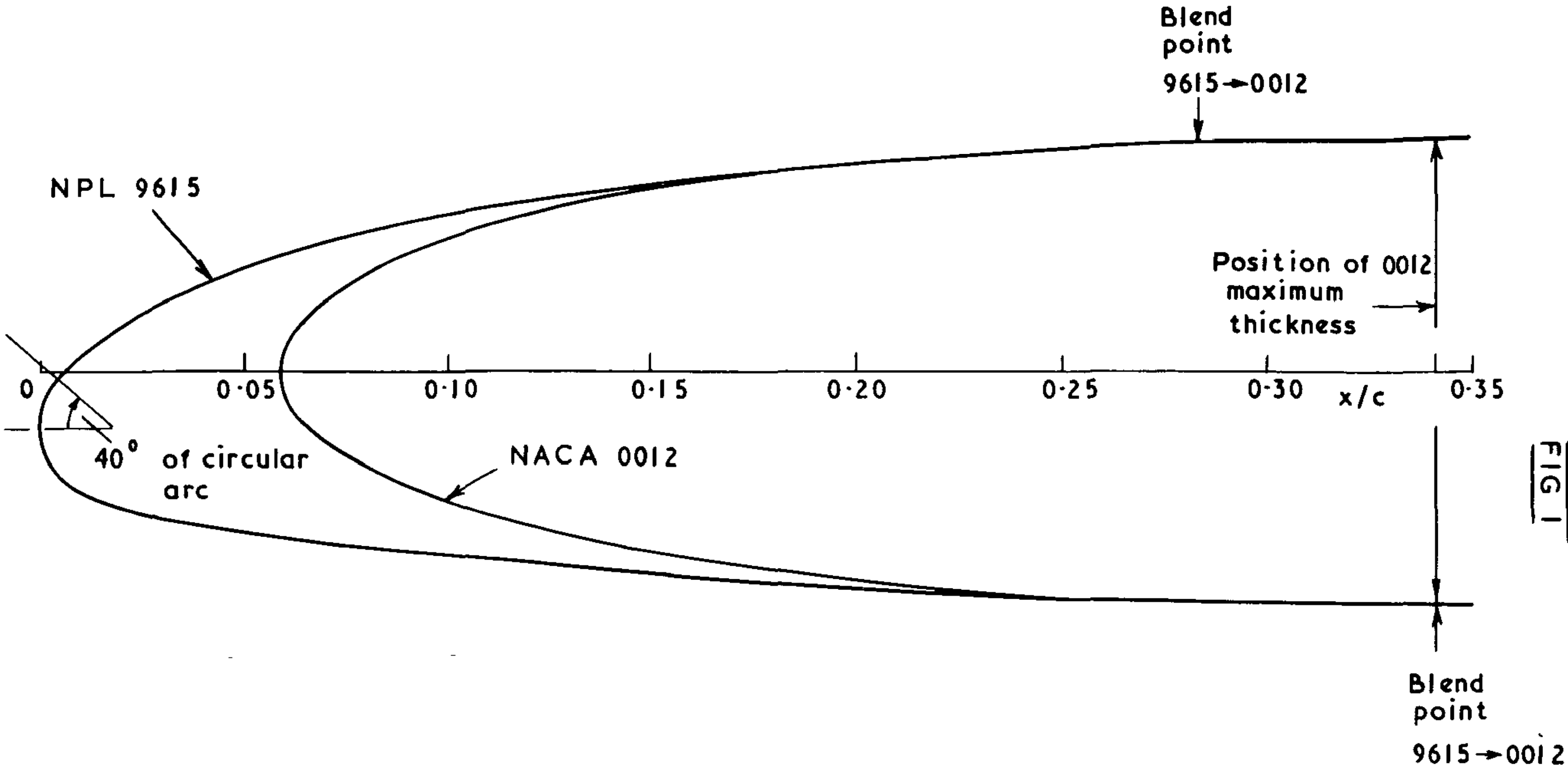

30657
FIG 1

Comparison of profiles ahead of position of maximum thickness

30657

FIG 2

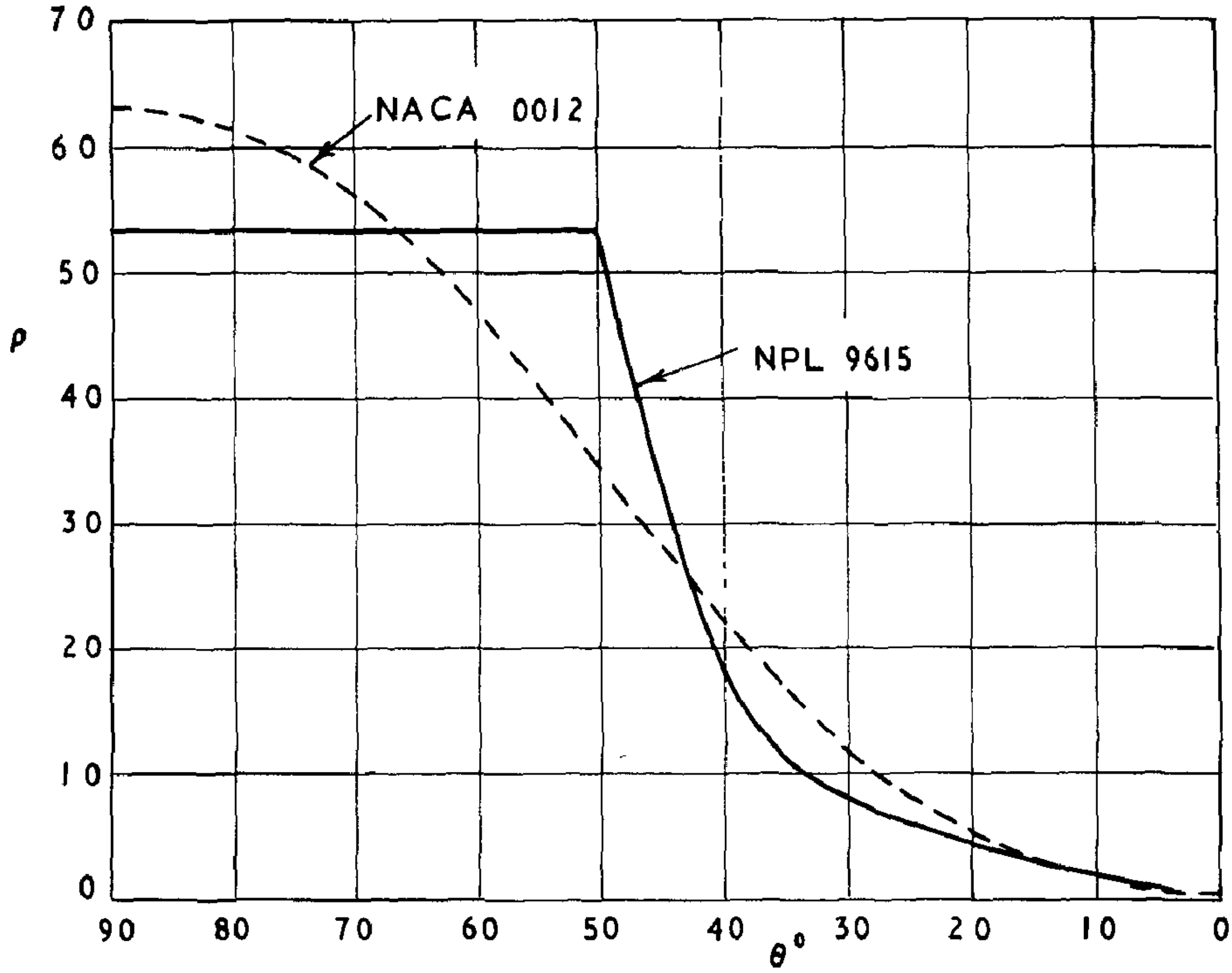

Comparison of upper surface curvature distributions

(ρ non-dimensionalised on actual chord)

30657
FIG. 3

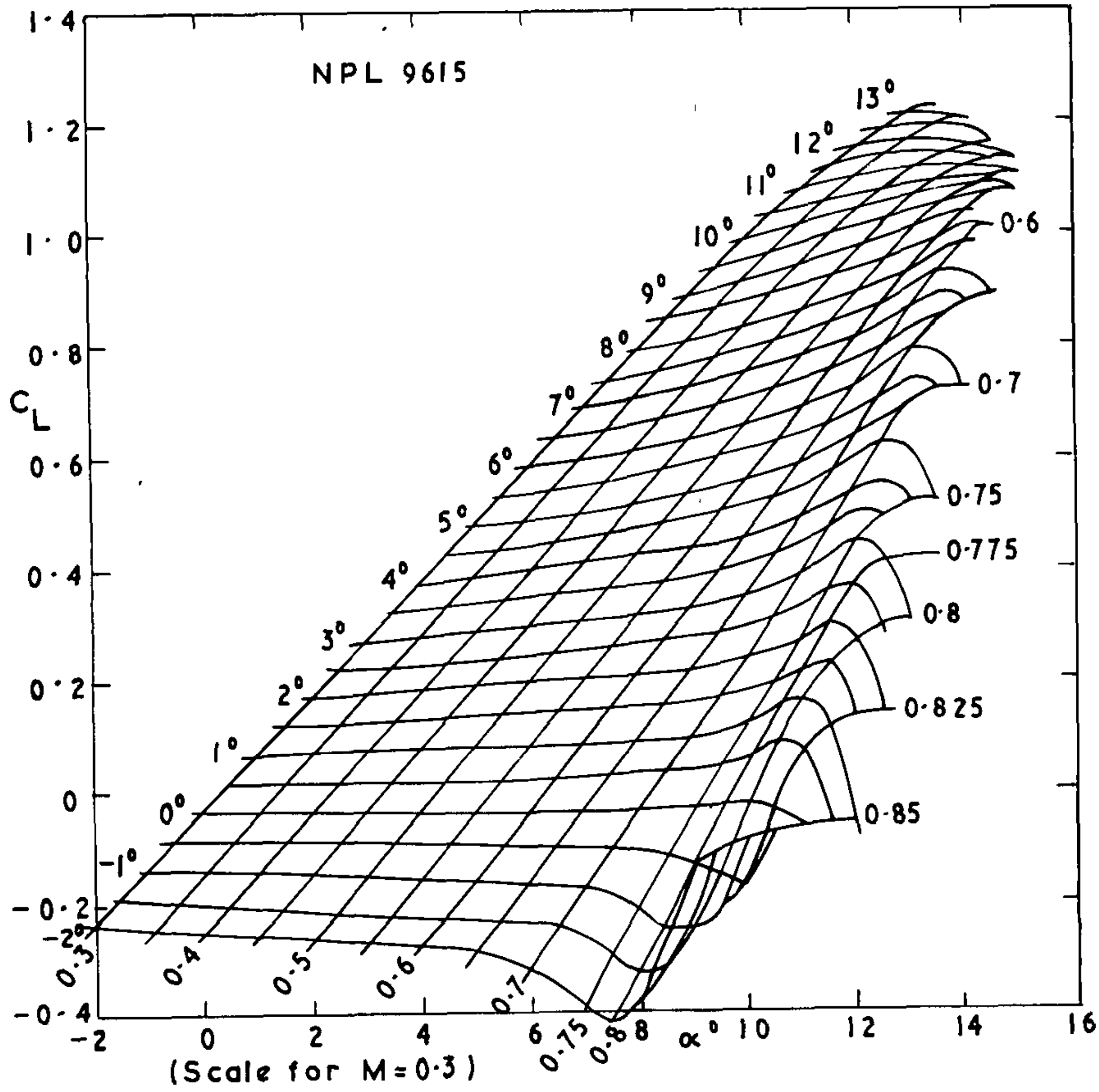

Variation of C_L with α and M for NPL 9615

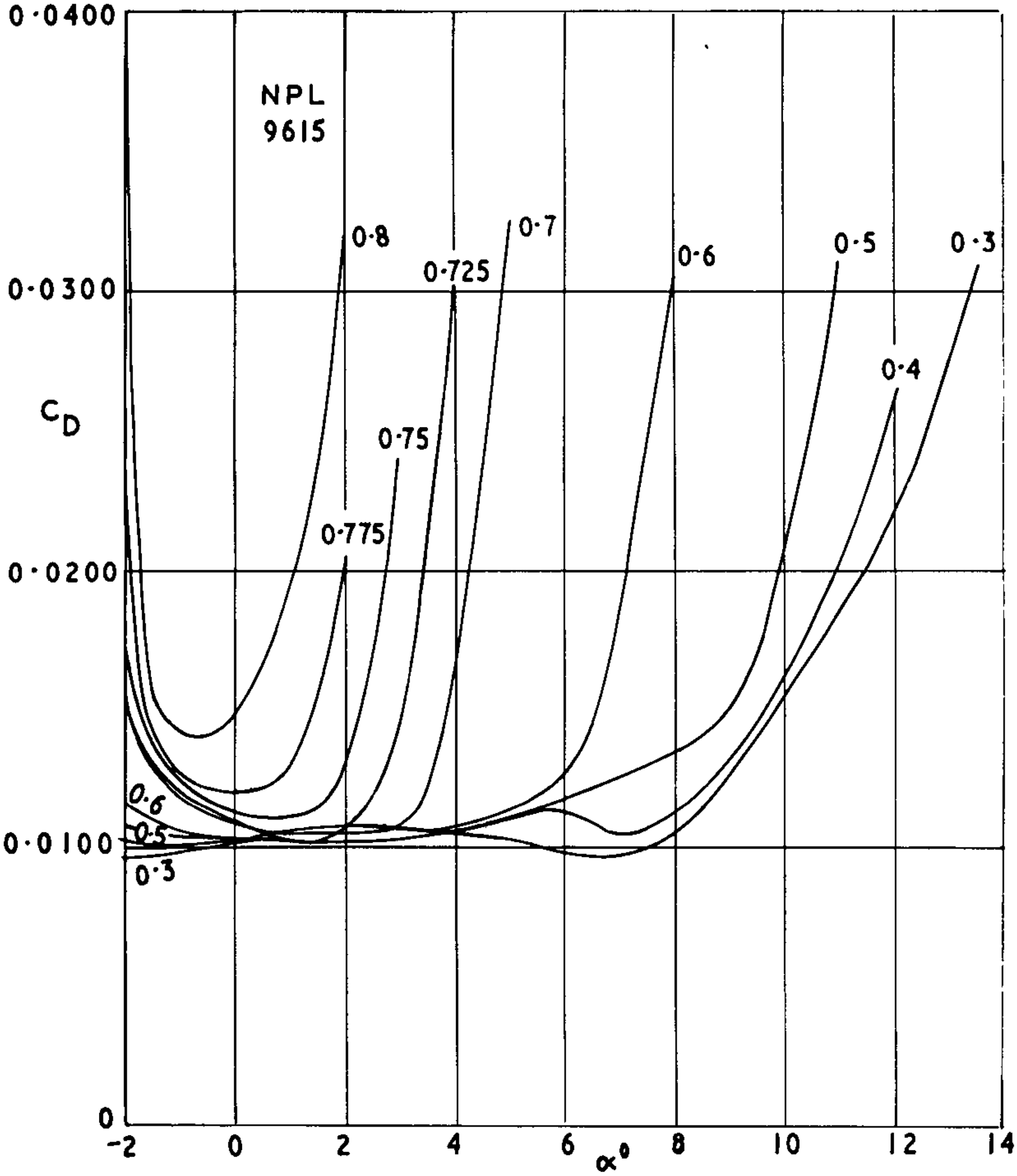

Variation of C_D with α and M for NPL 9615

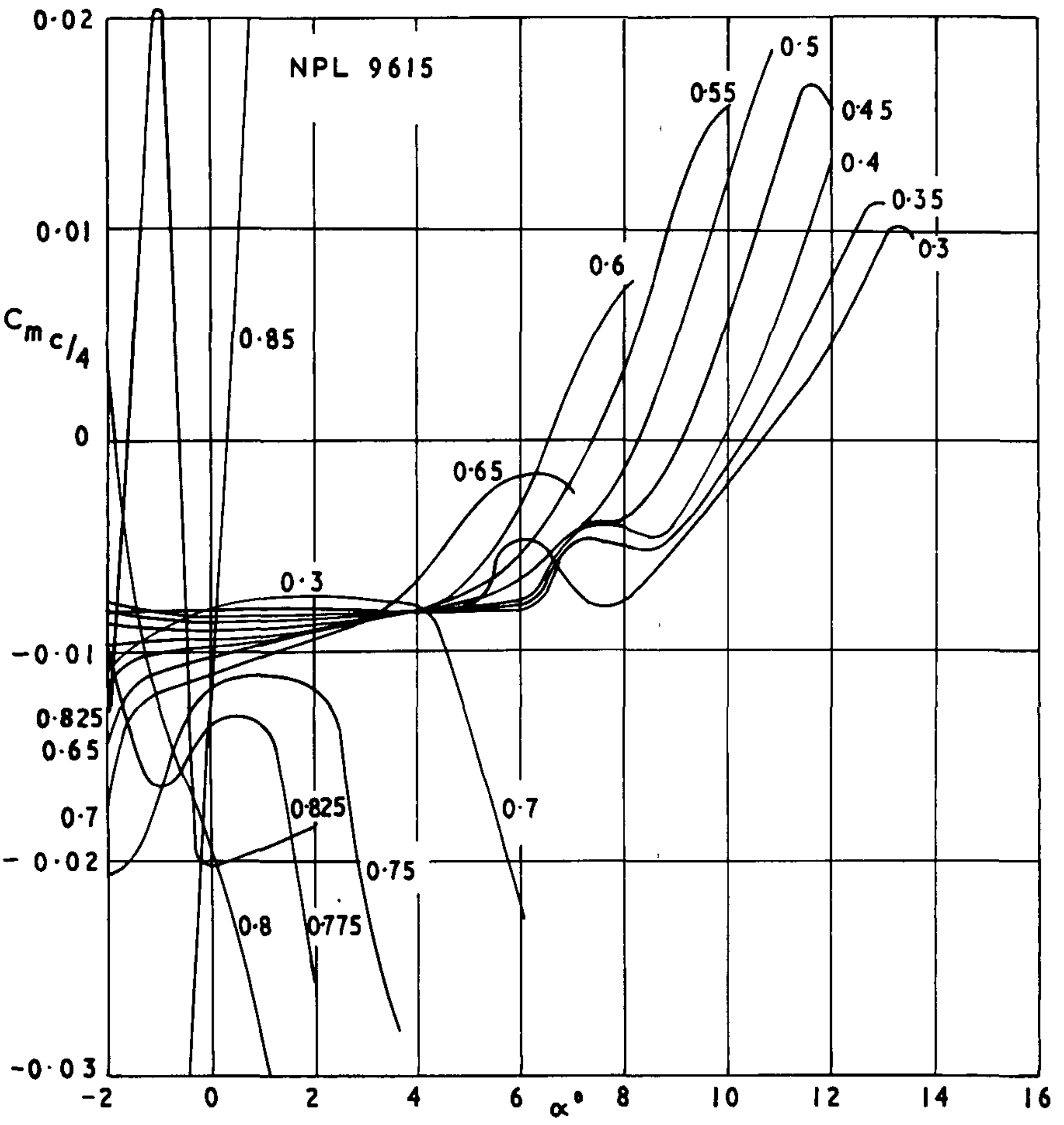

Variation of $C_{m\,c/4}$ with α and M for NPL 9615

30657
FIG. 6

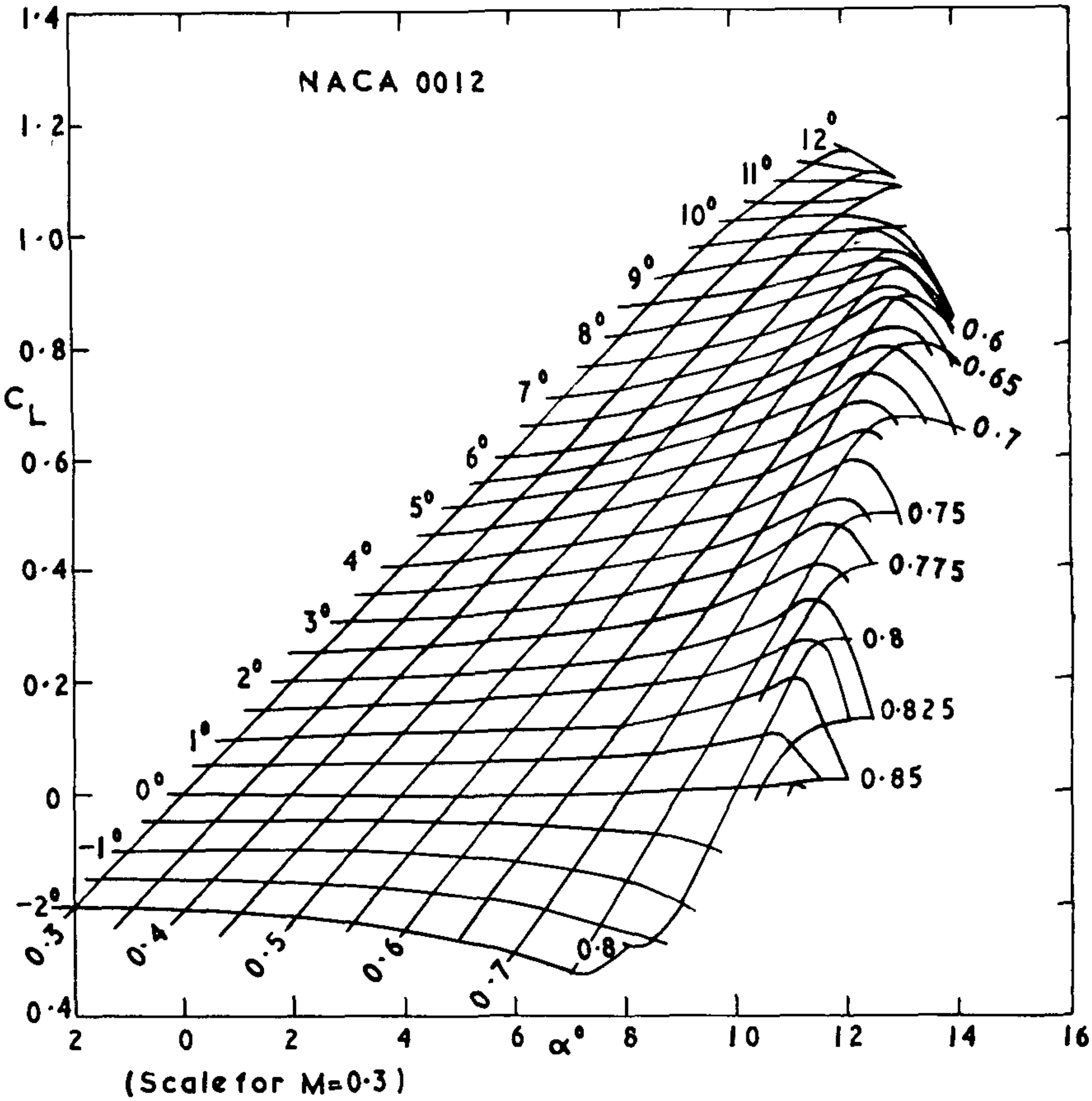

Variation of C_L with α and M for NACA 0012

FIG. 7

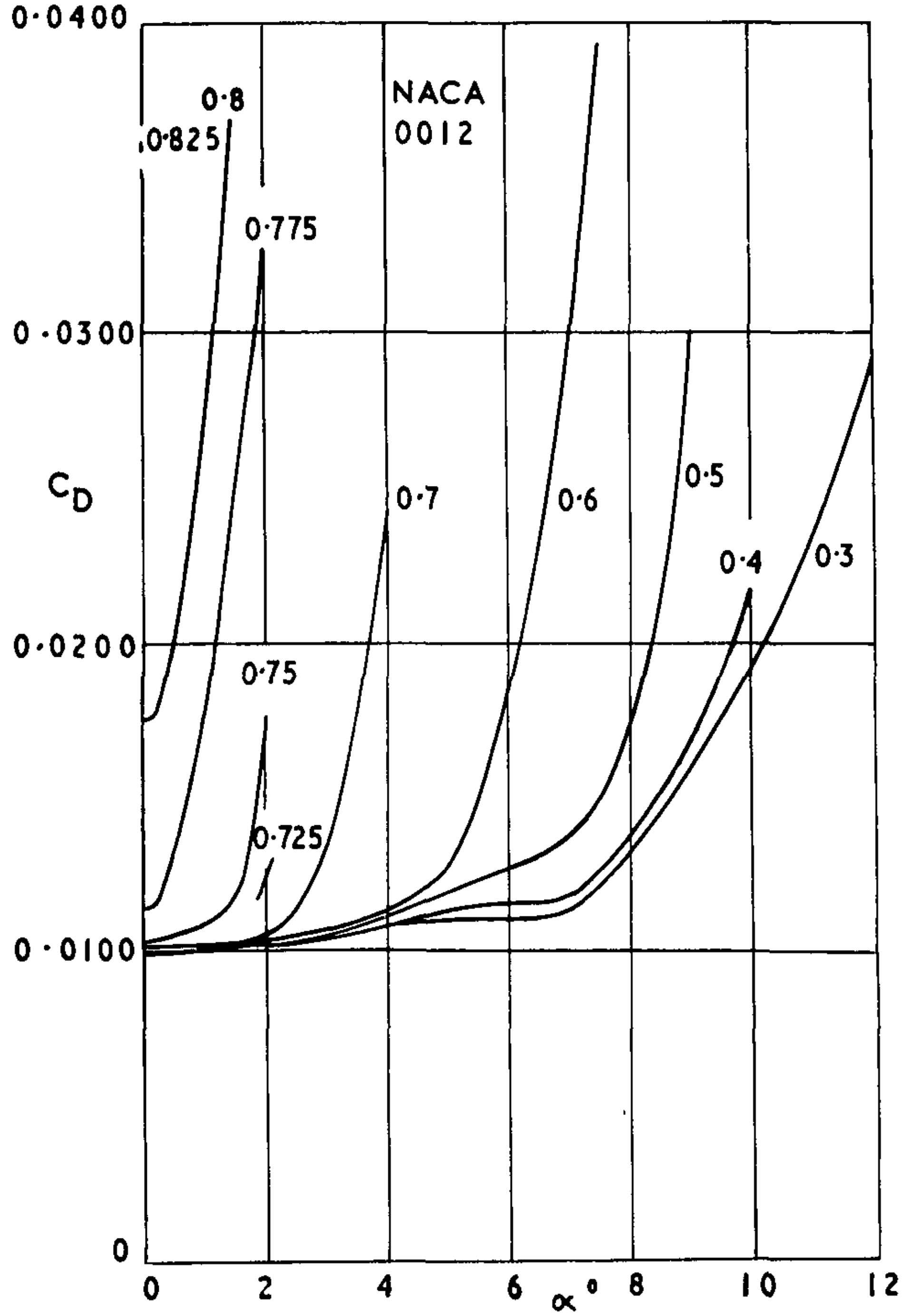

Variation of C_D with α and M for NACA 0012

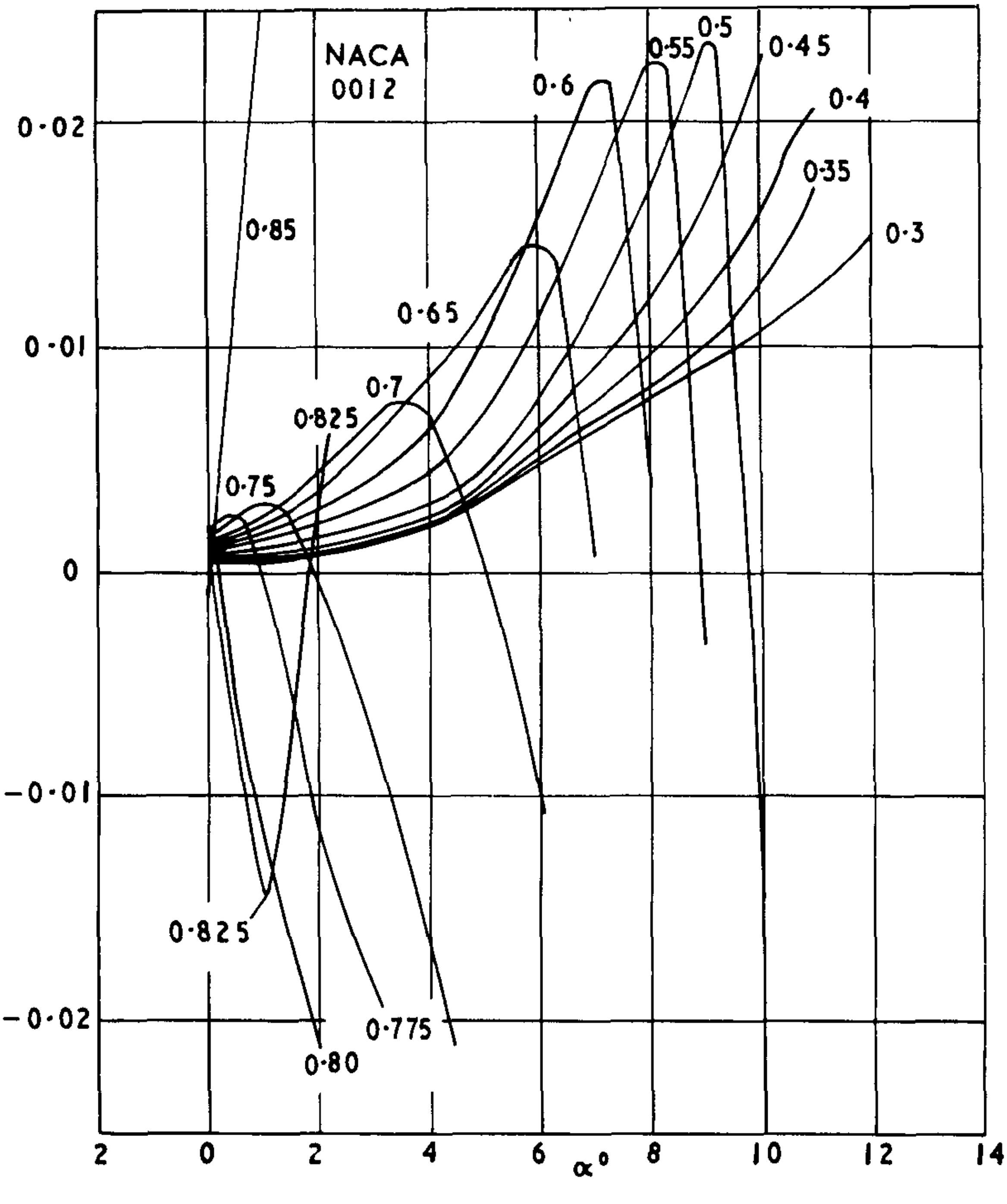

Variation of $C_{m_{c/4}}$ with α and M for NACA 0012

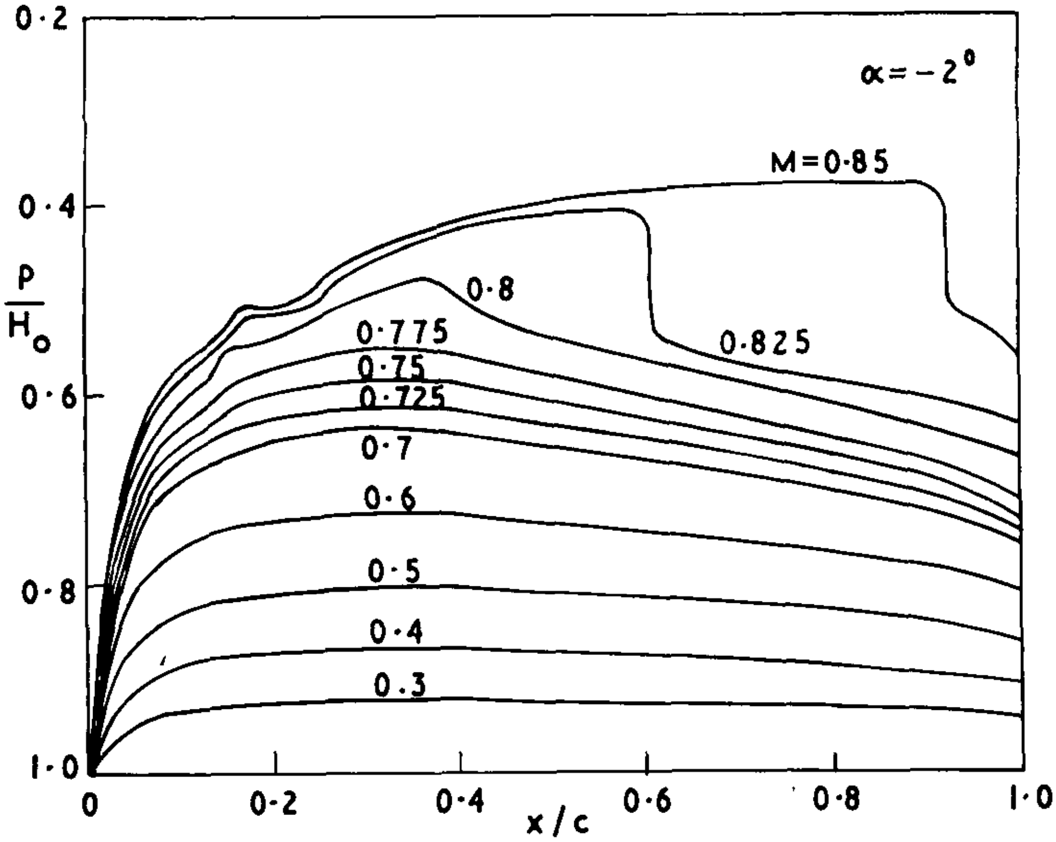

Upper surface

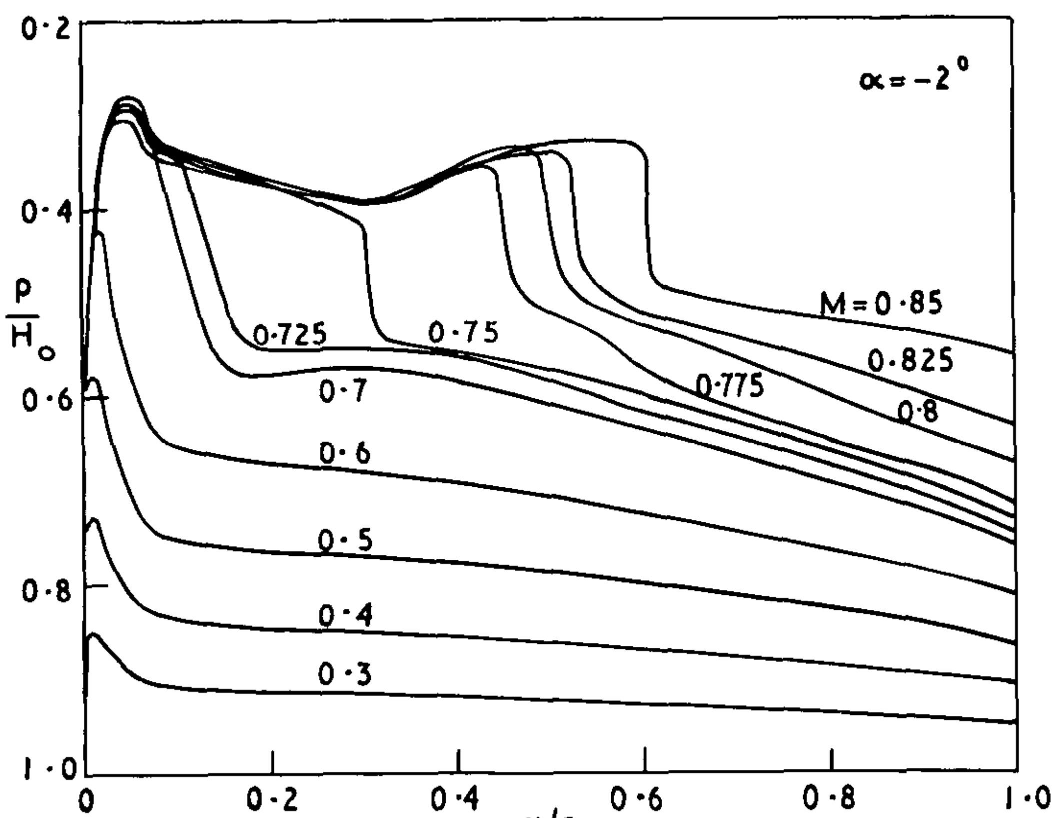

Lower surface

NPL 9615 Pressure distributions, $\alpha = -2^{\circ}$

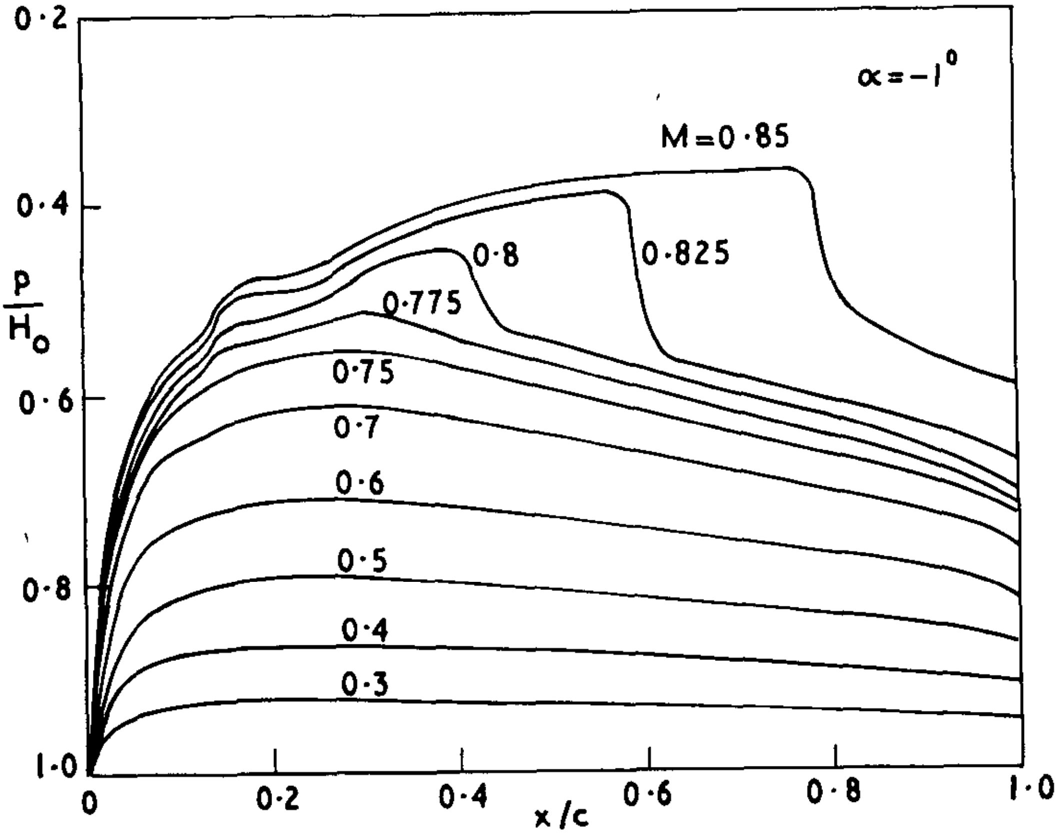

Upper surface

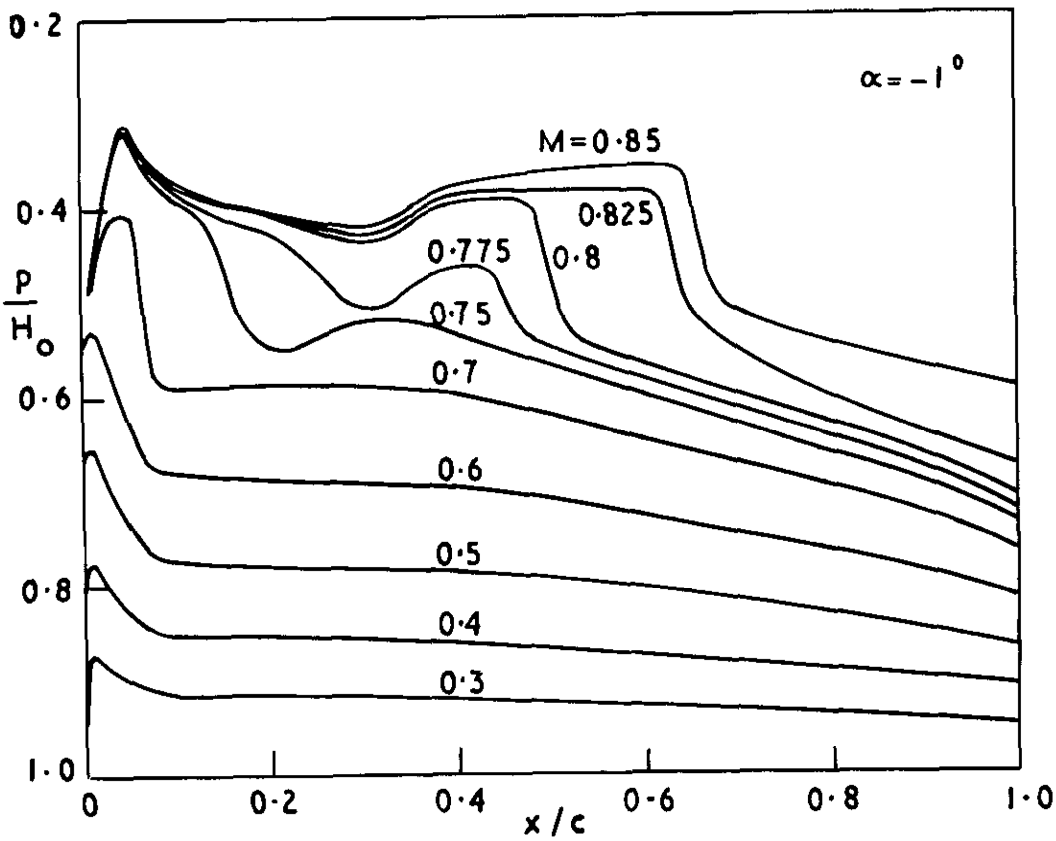

Lower surface

NPL 9615 Pressure distributions, α = -1°

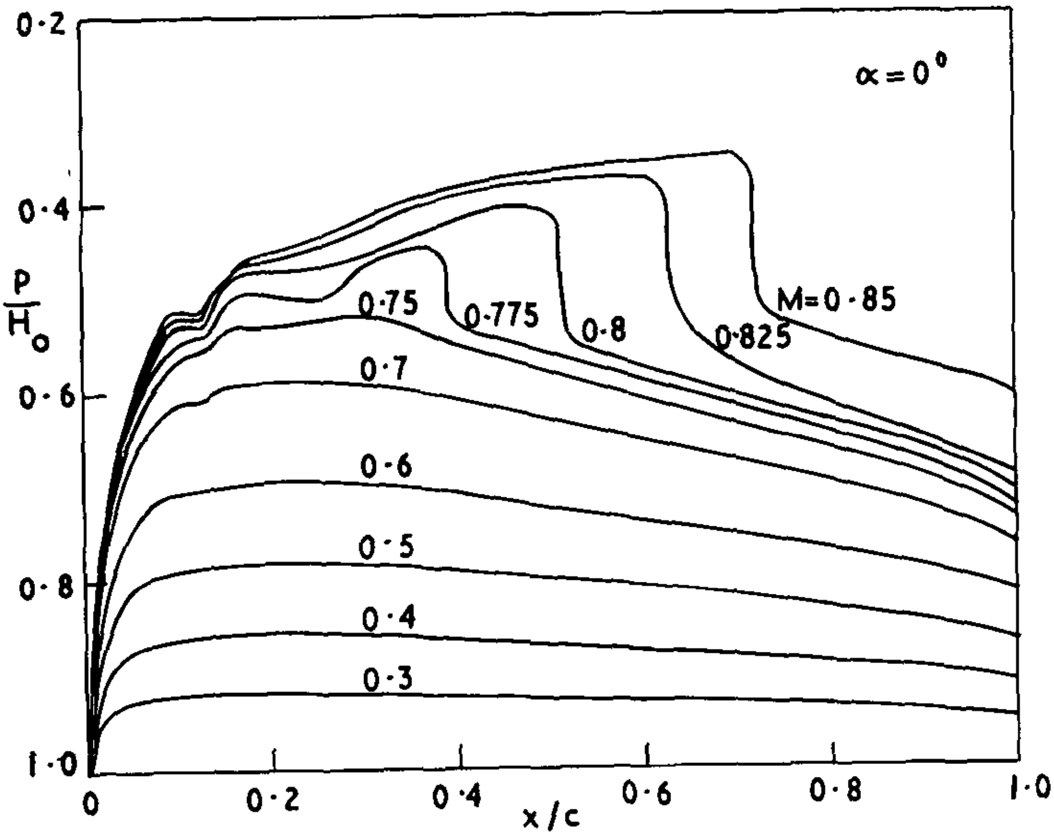

Upper surface

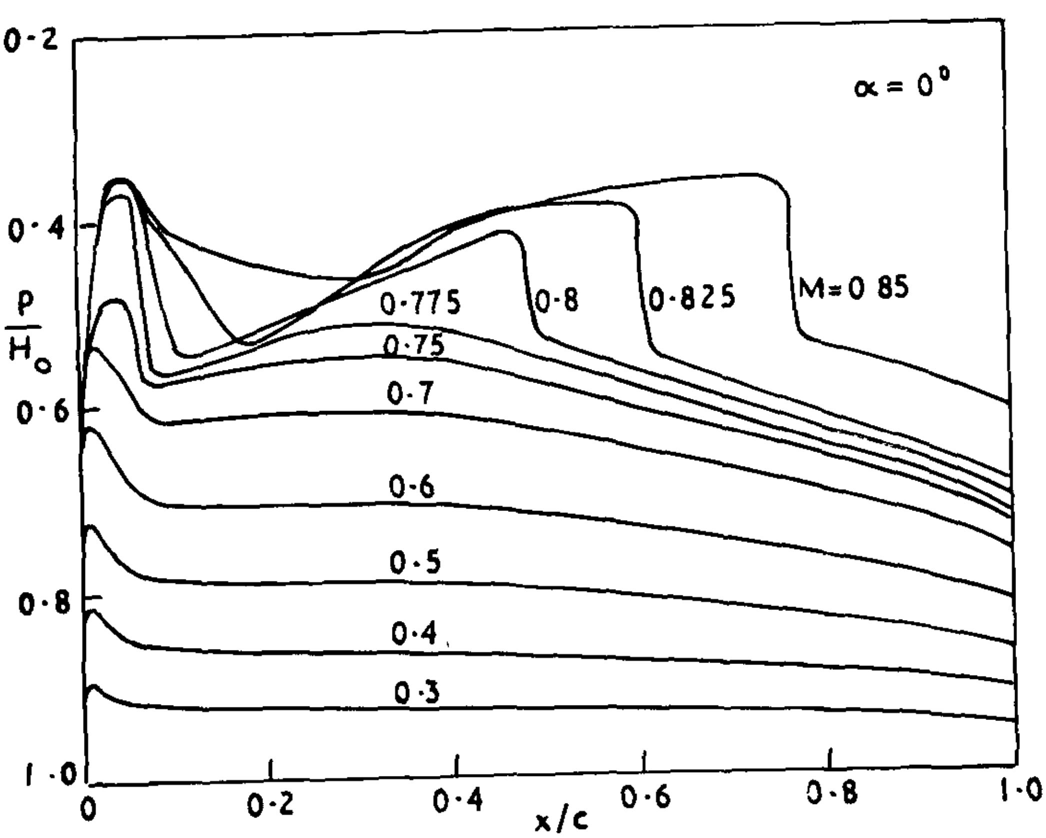

Lower surface

NPL 9615 Pressure distributions, $\alpha = 0°$

30657

FIG. 9d

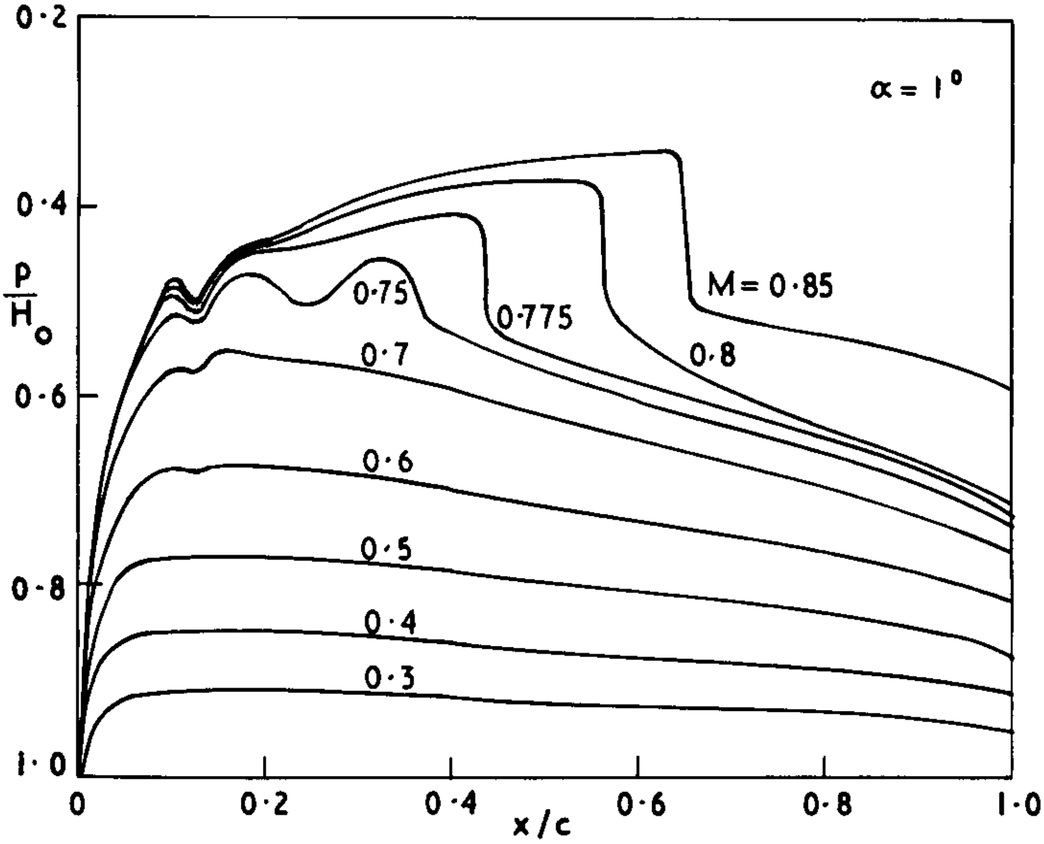

Upper surface

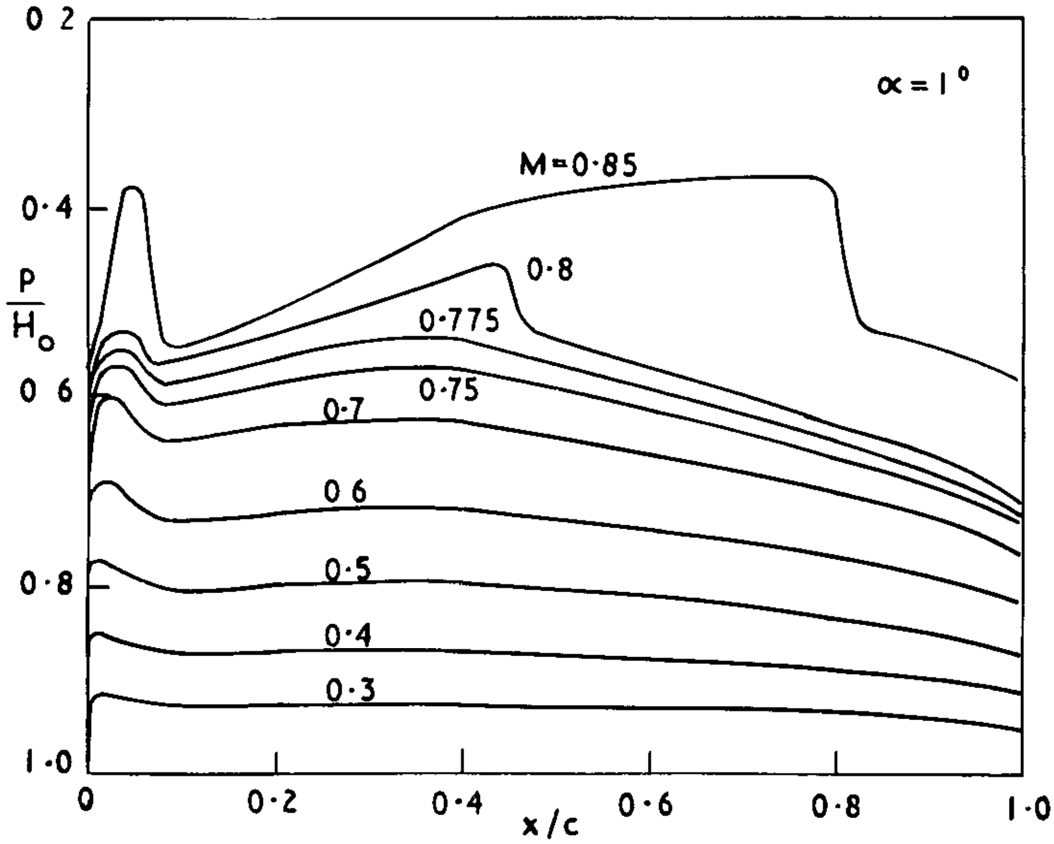

Lower surface

NPL 9615 Pressure distributions $\alpha = 1^\circ$

FIG. 9e

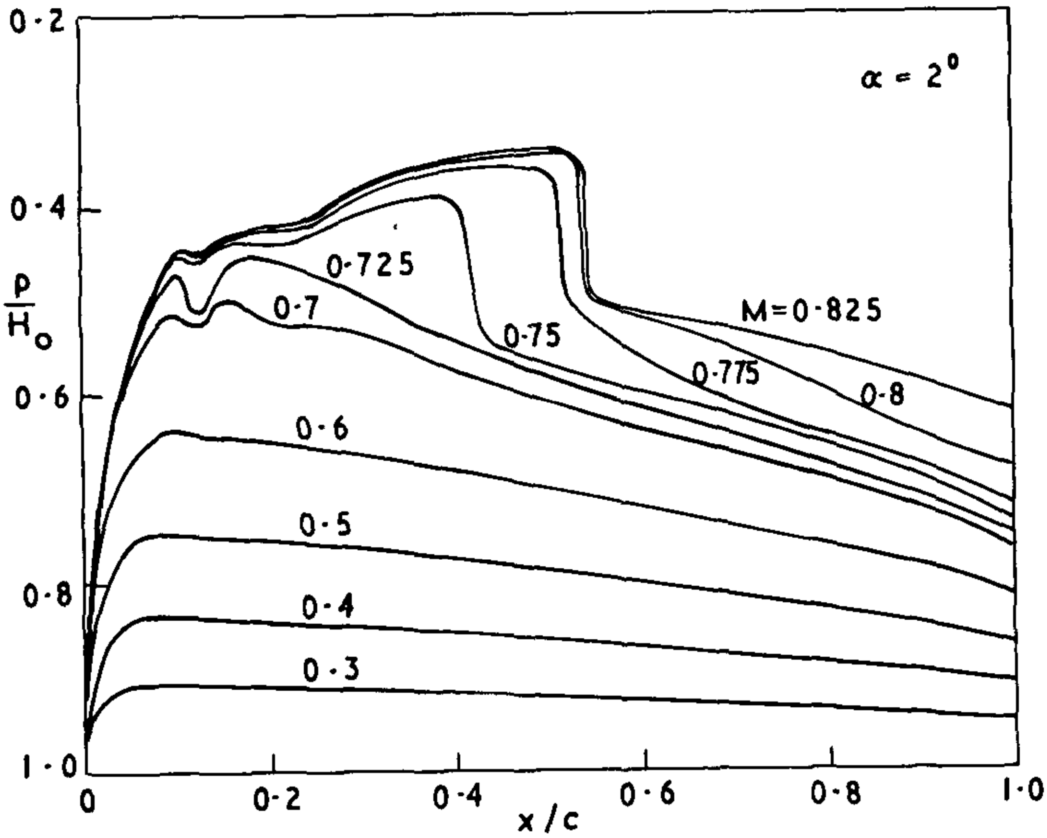

Upper surface

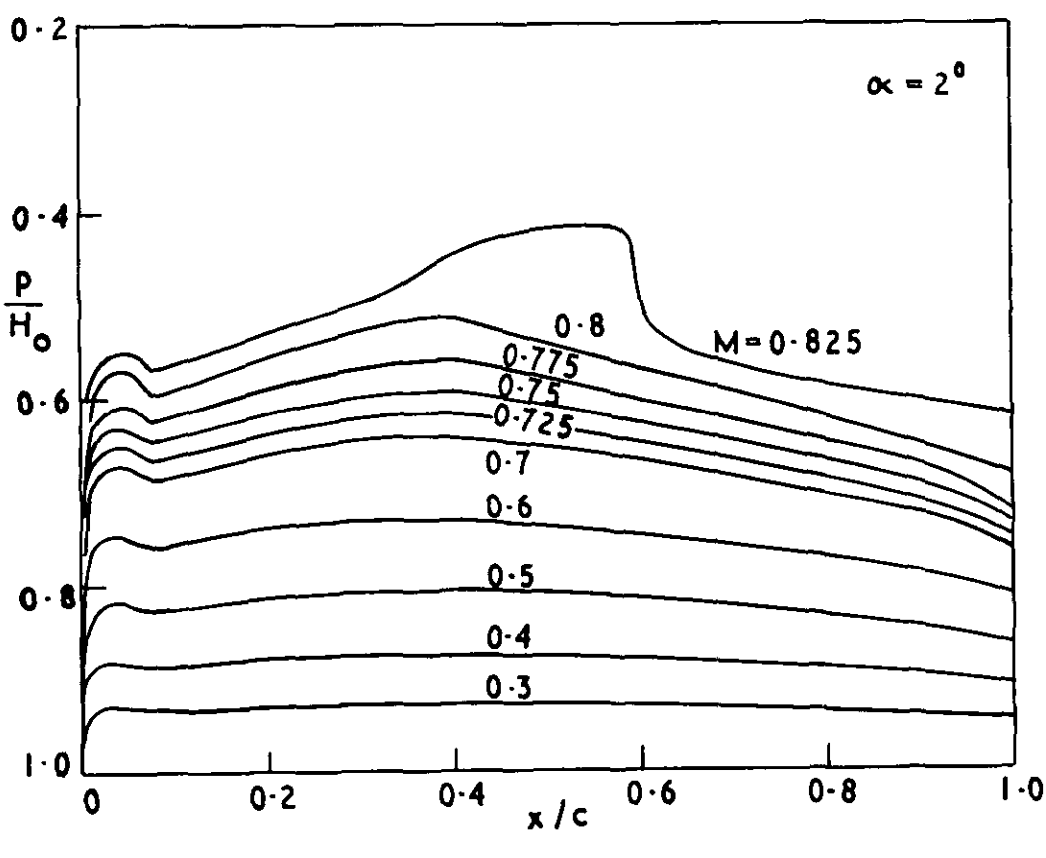

Lower surface

NPL 9615 Pressure distributions, $\alpha = 2°$

30657

FIG. 9f

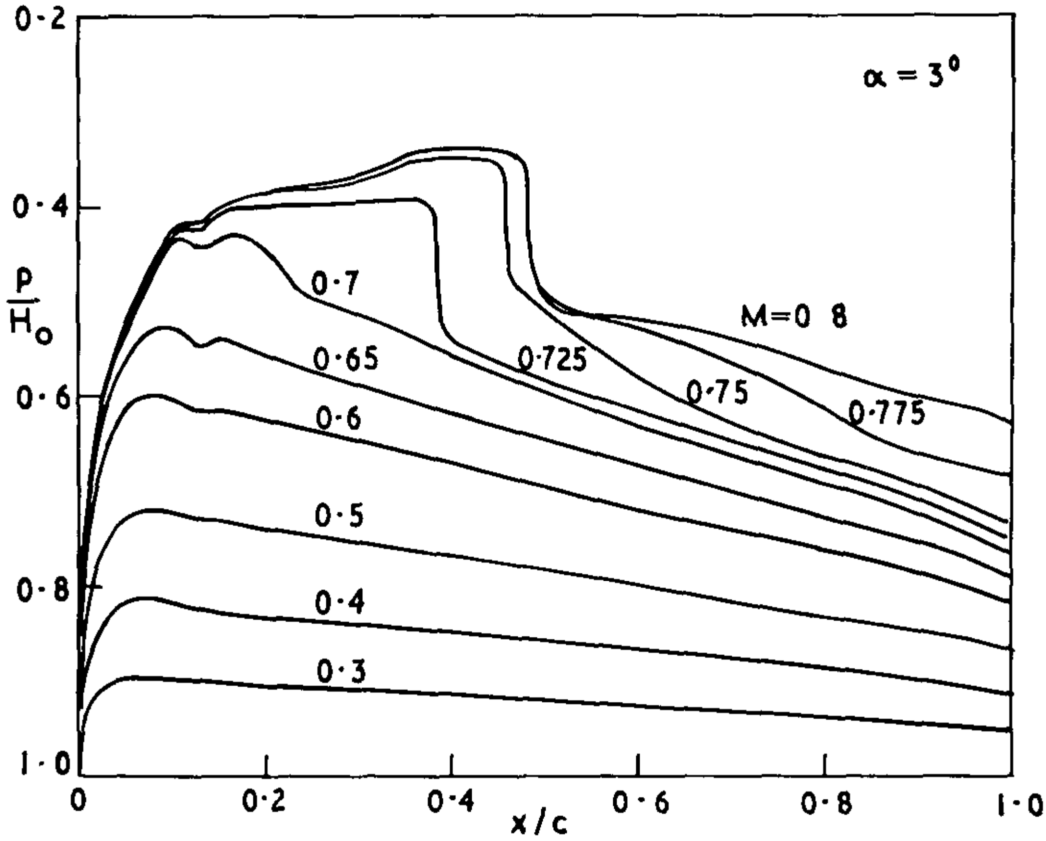

Upper surface

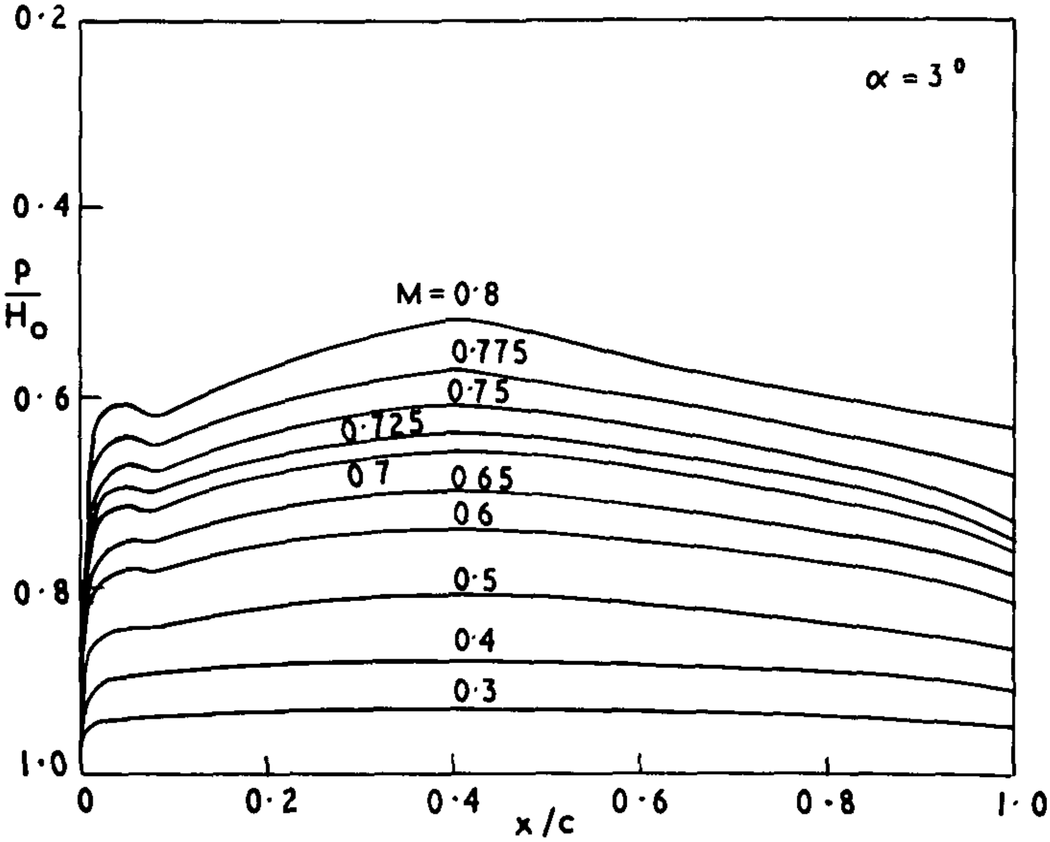

Lower surface

NPL 9615 Pressure distributions, $\alpha = 3^{\circ}$

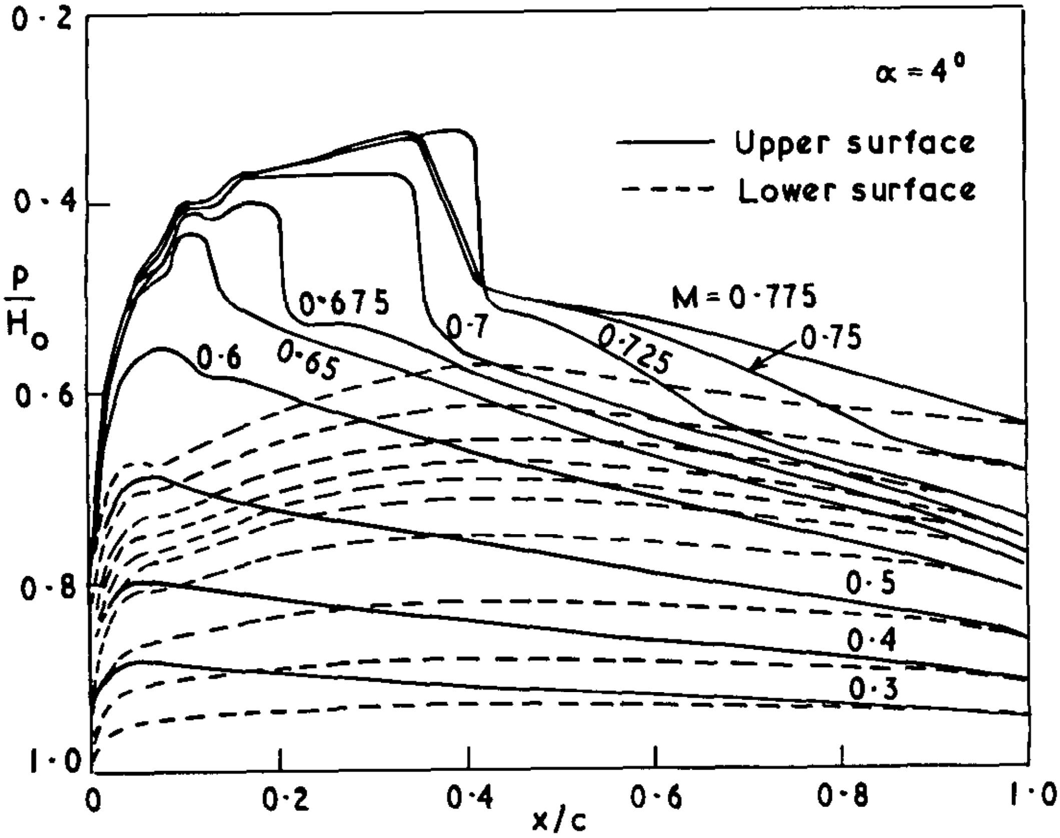

g NPL 9615 Pressure distributions, $\alpha = 4^\circ$

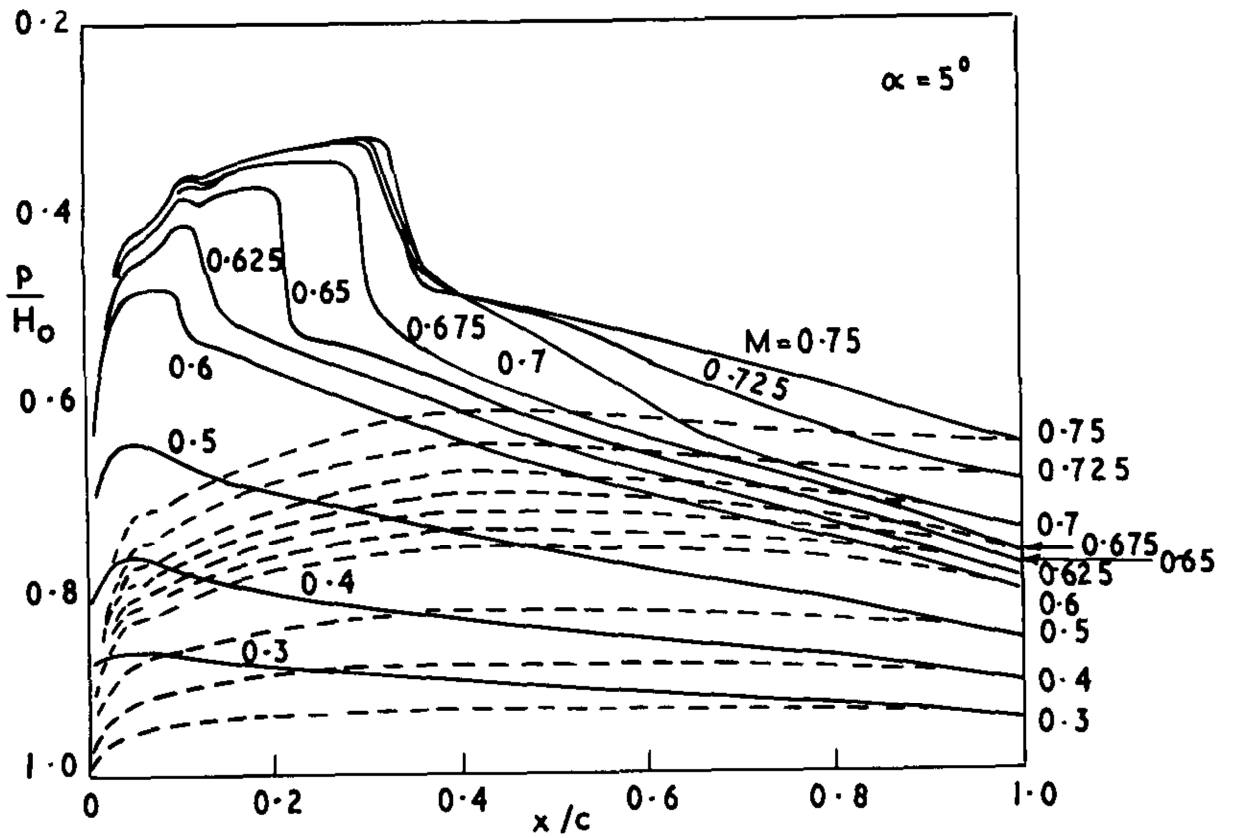

h NPL 9615 Pressure distributions, $\alpha = 5^\circ$

30657
FIG. 9 i & j

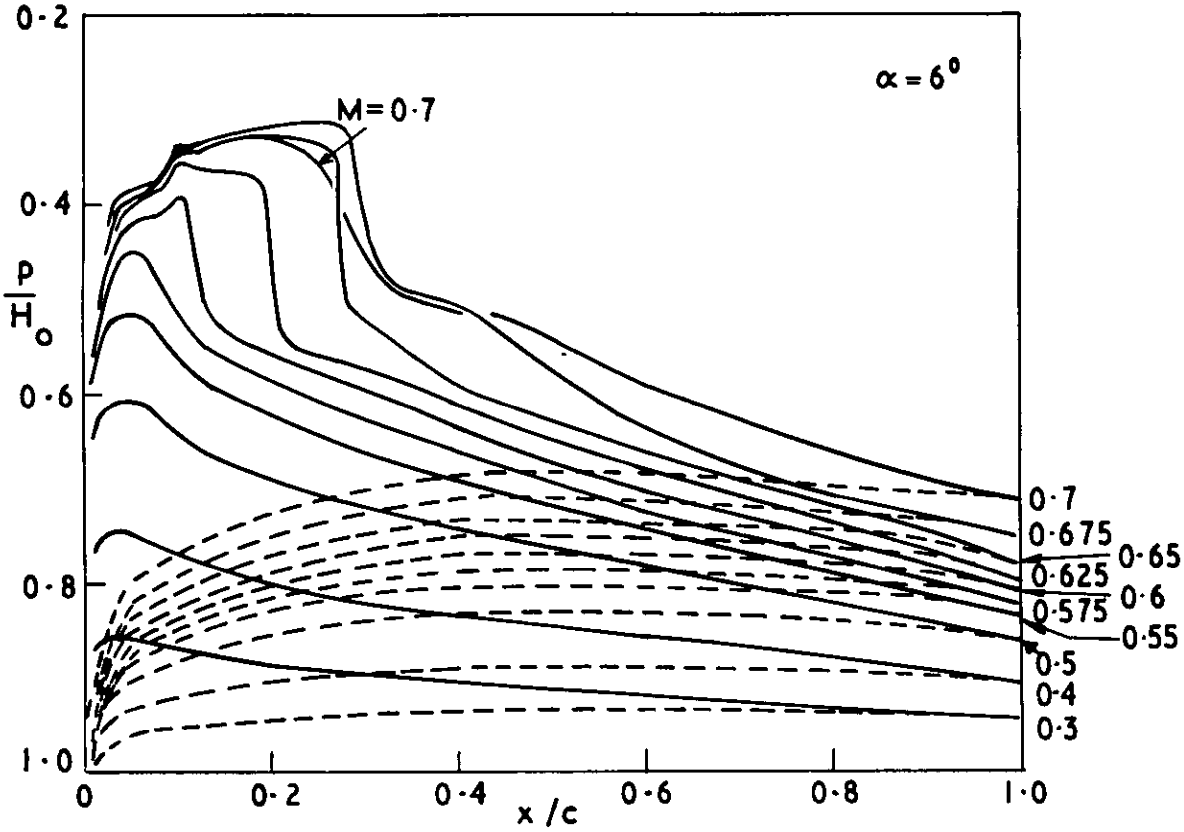

i NPL 9615 Pressure distributions, $\alpha = 6^\circ$

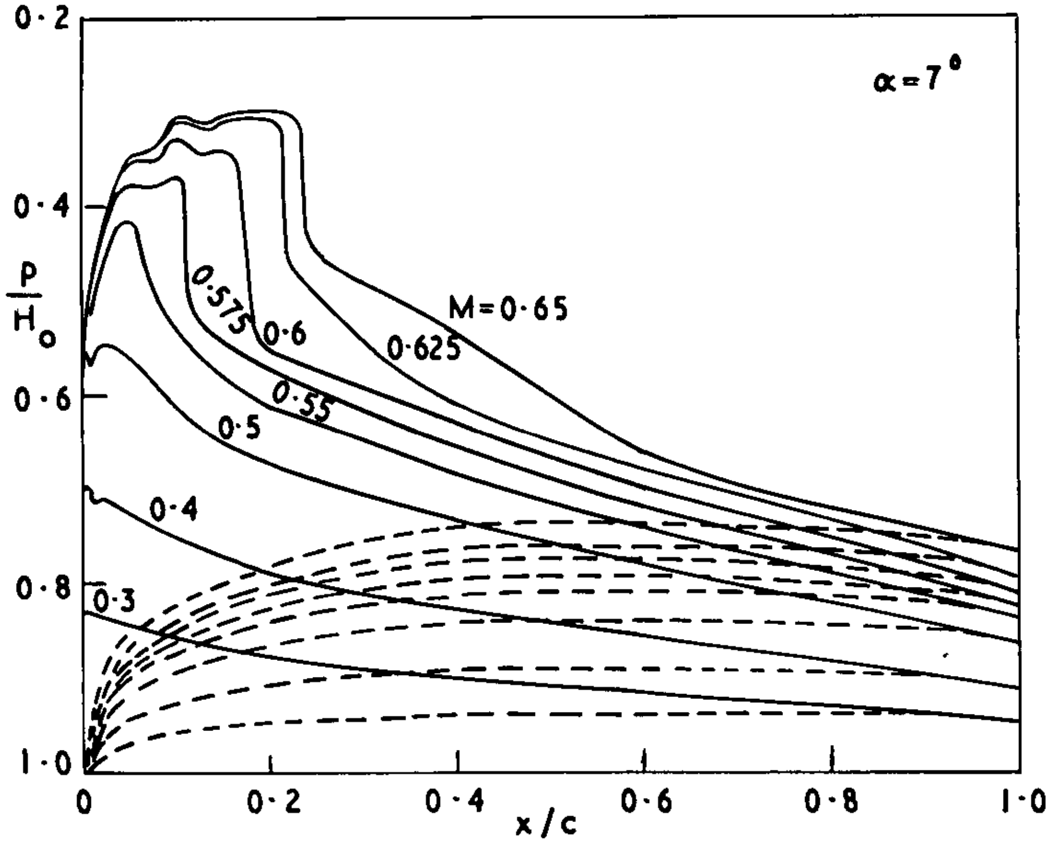

j NPL 9615 Pressure distributions, $\alpha = 7^\circ$

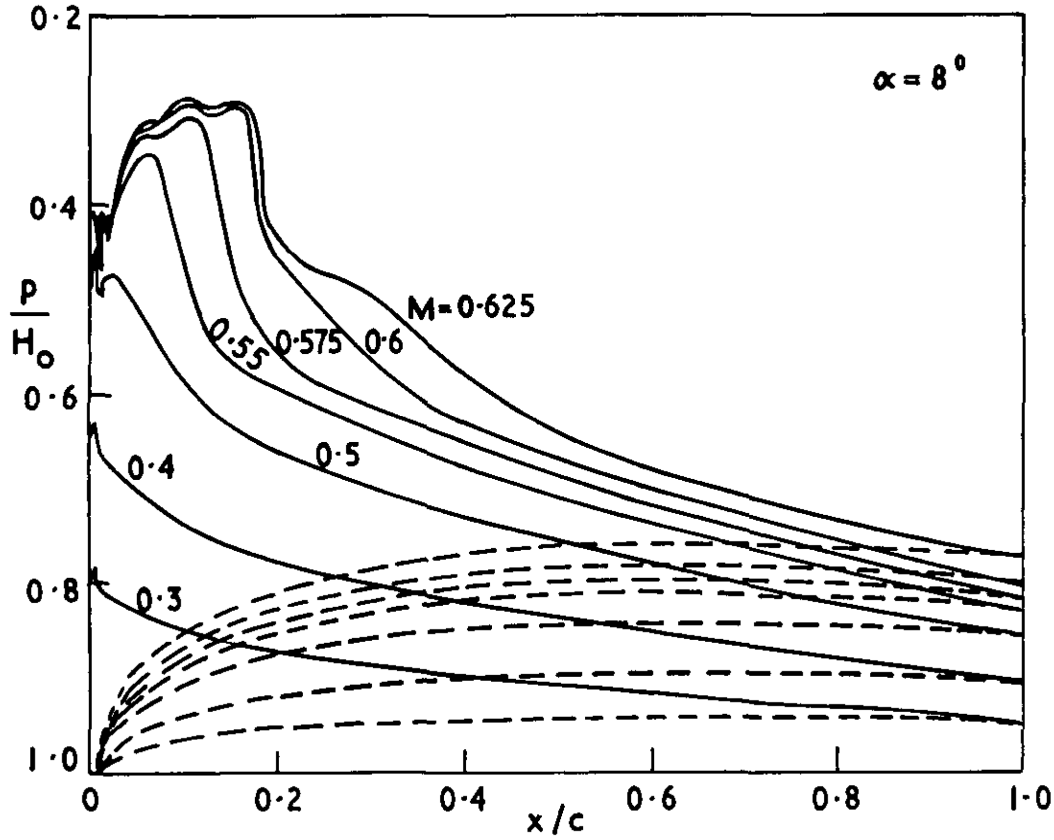

k NPL 9615 Pressure distributions, $\alpha = 8^\circ$

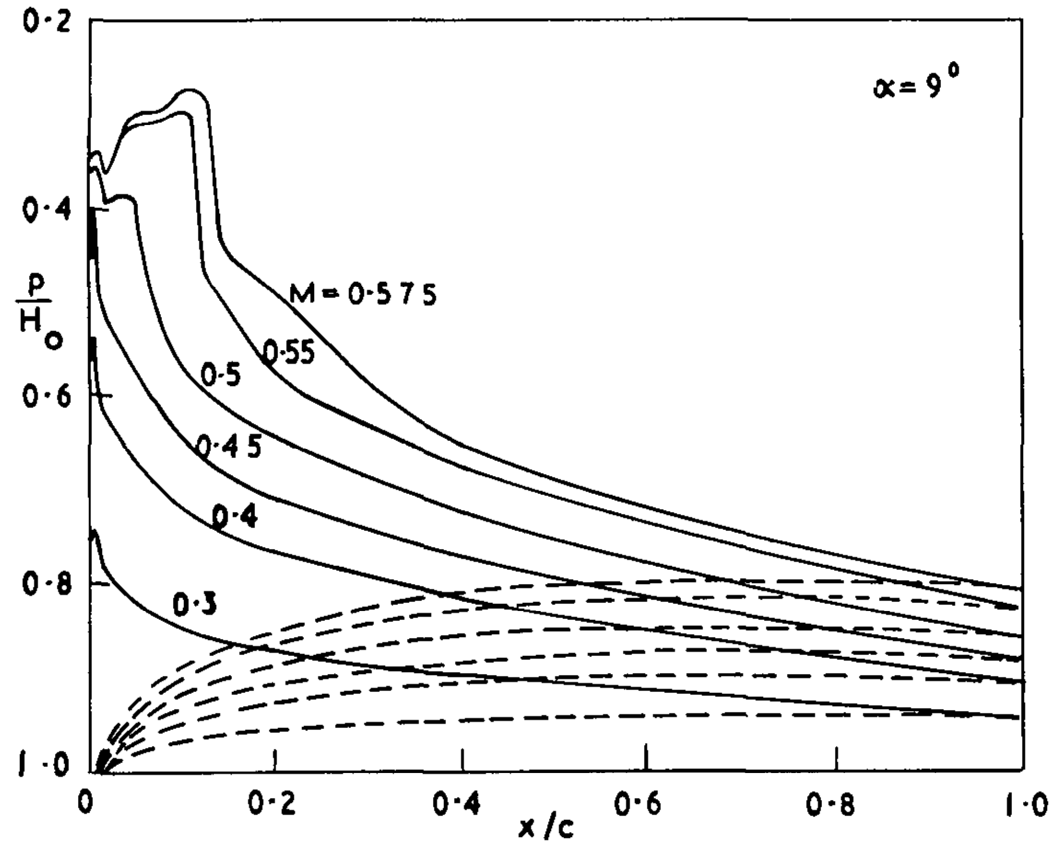

l NPL 9615 Pressure distributions, $\alpha = 9^\circ$

30657
FIG. 9m

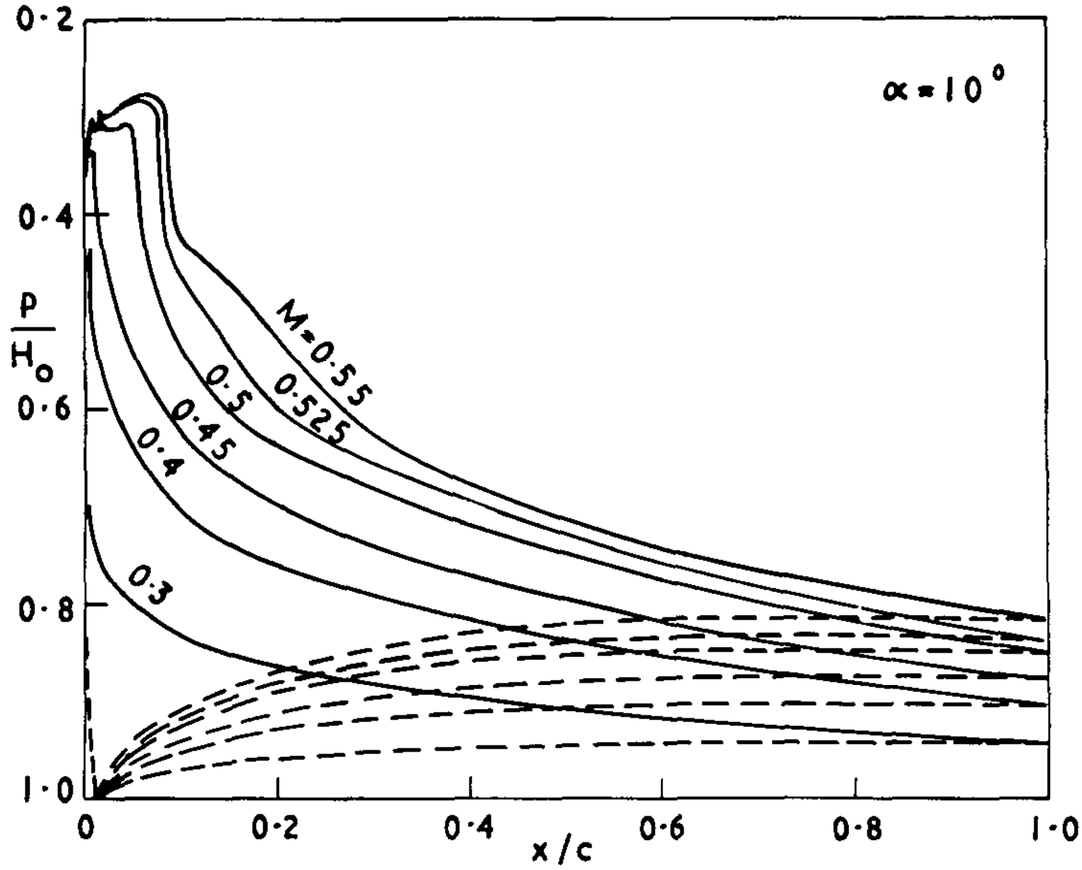

m NPL 9615 Pressure distributions, α = 10°

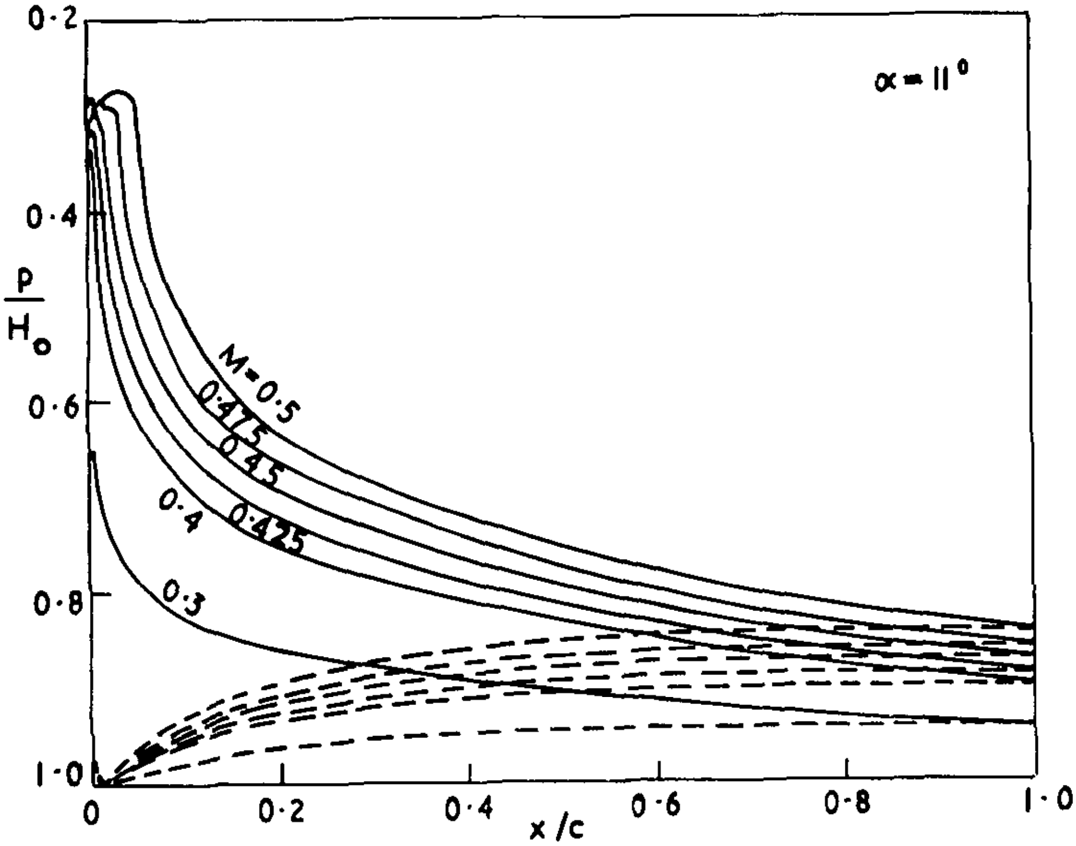

n NPL 9615 Pressure distribution α = 11°

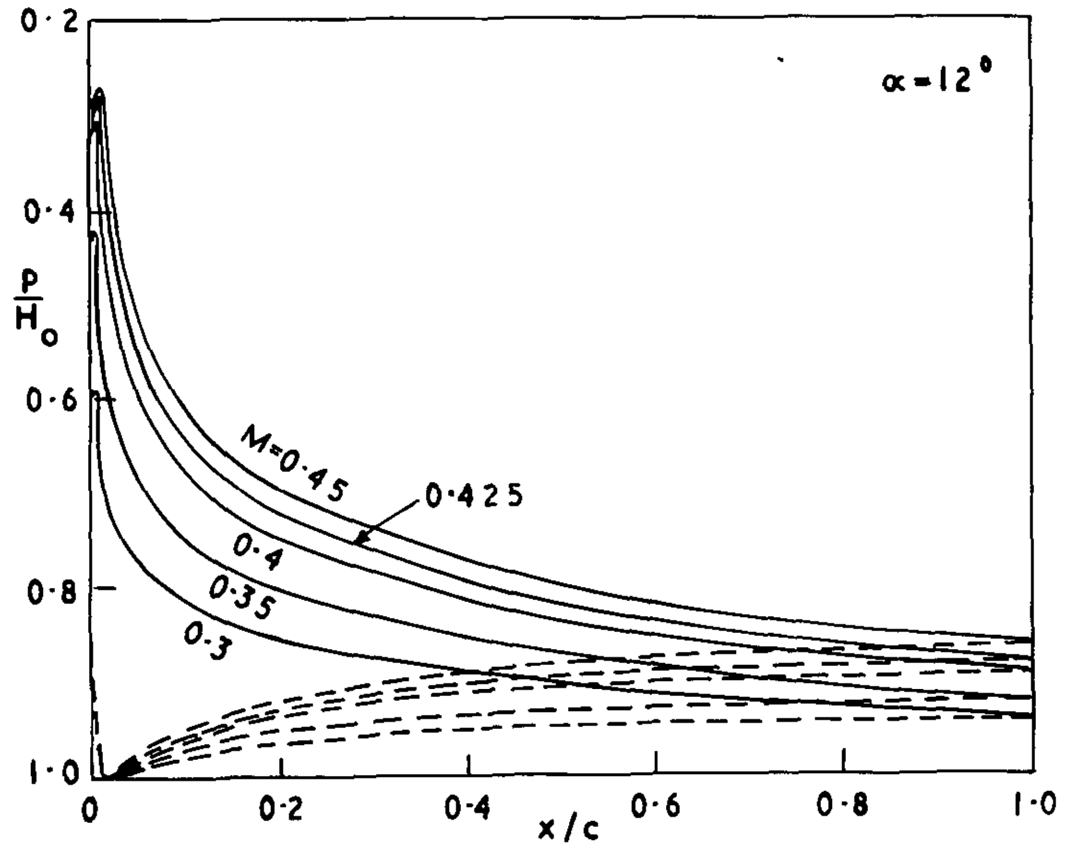

o NPL 9615 Pressure distributions, α = 12°

FIG 9p &q.

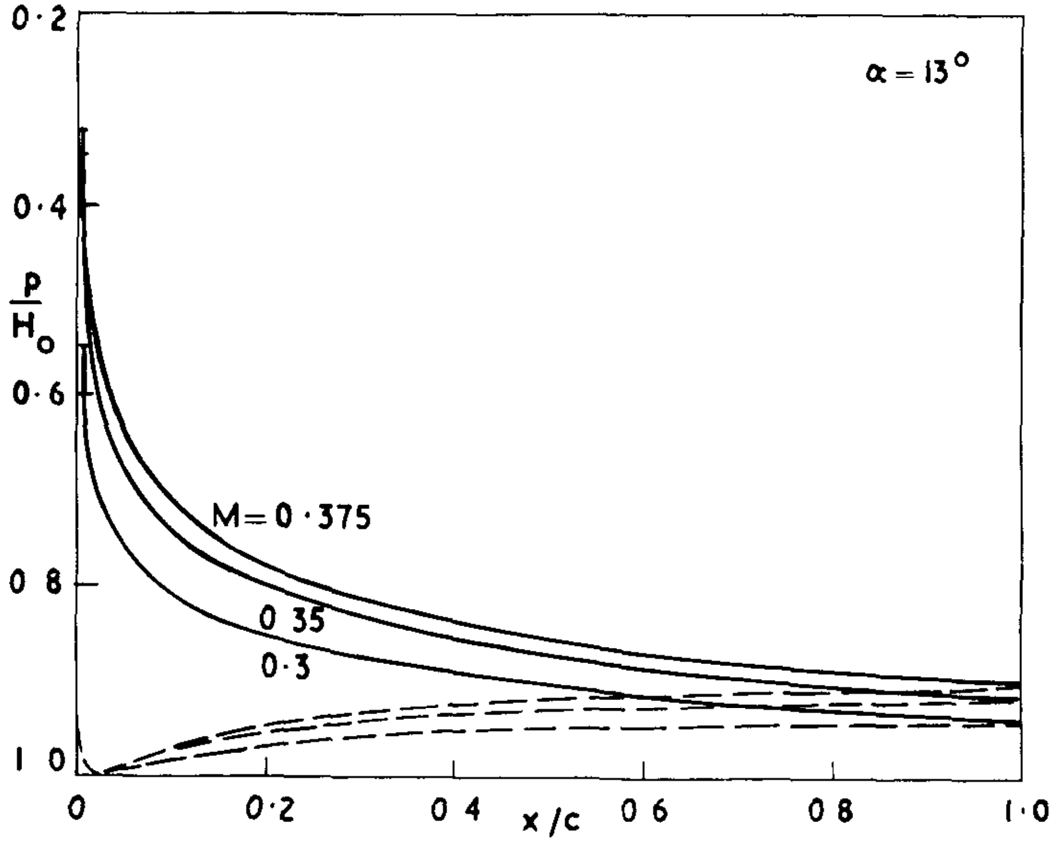

p NPL 9615 Pressure distributions. α = 13°

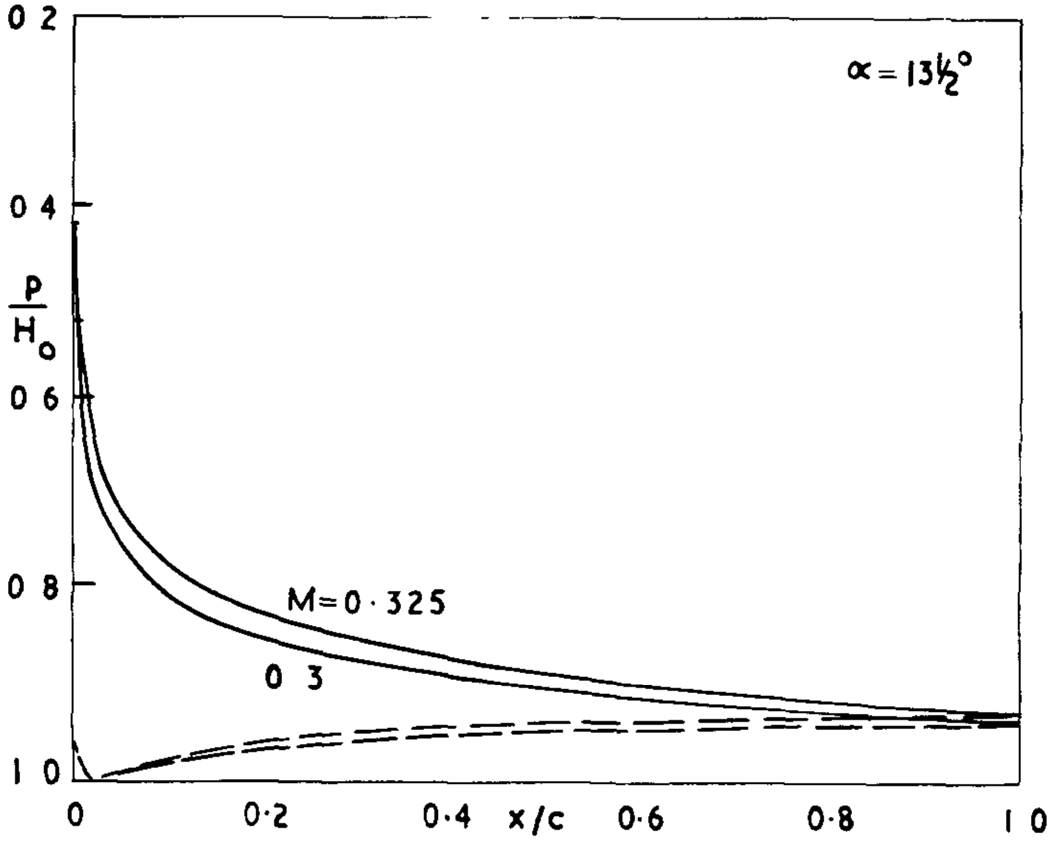

q NPL 9615 Pressure distributions, α = 13½°

30657
FIG 10 a & b

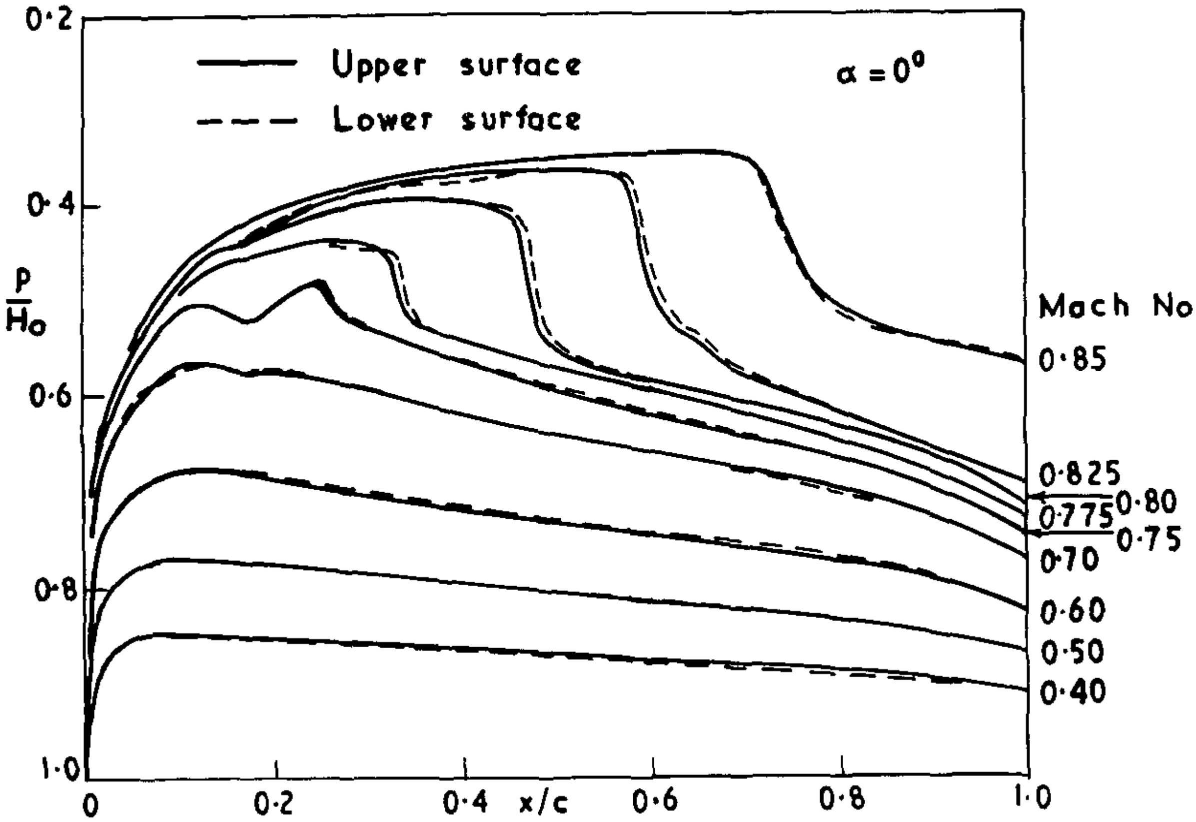

a NACA 0012 Pressure distributions, α = 0°

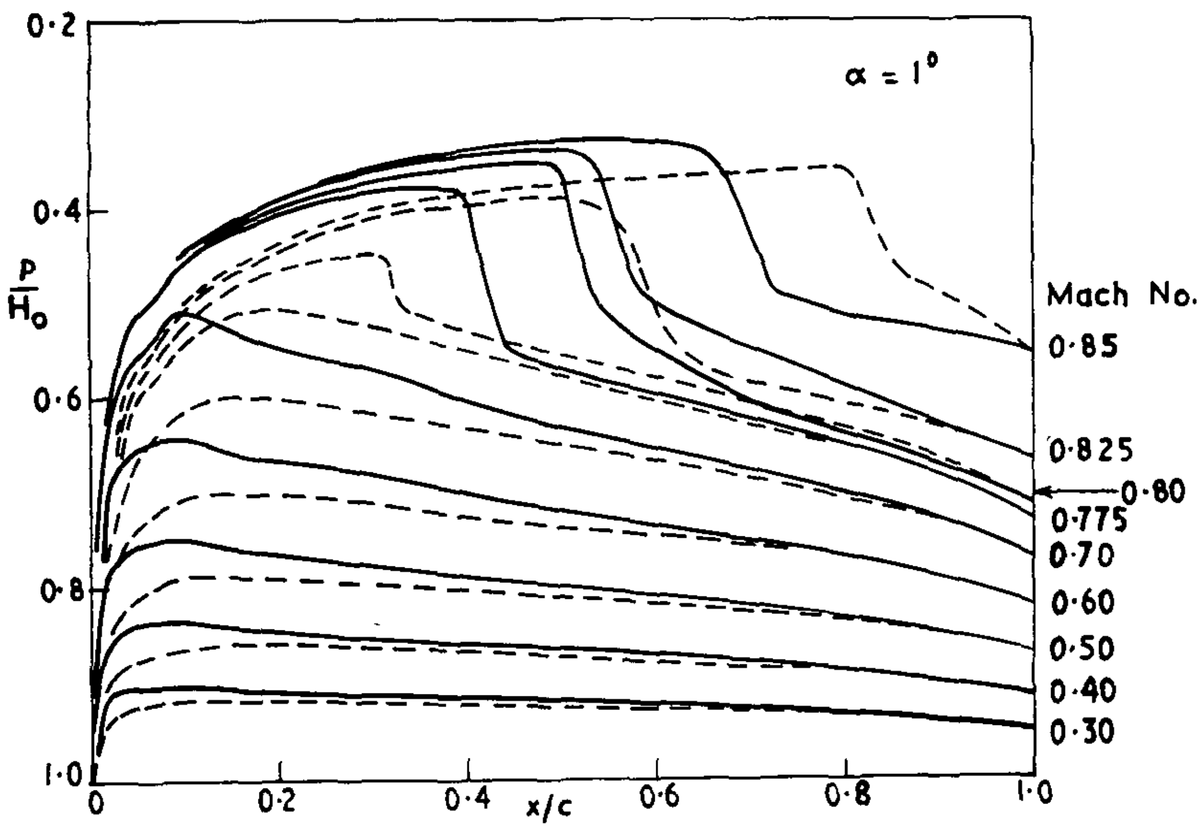

b NACA 0012 Pressure distributions, α = 1°

FIG.10 c & d

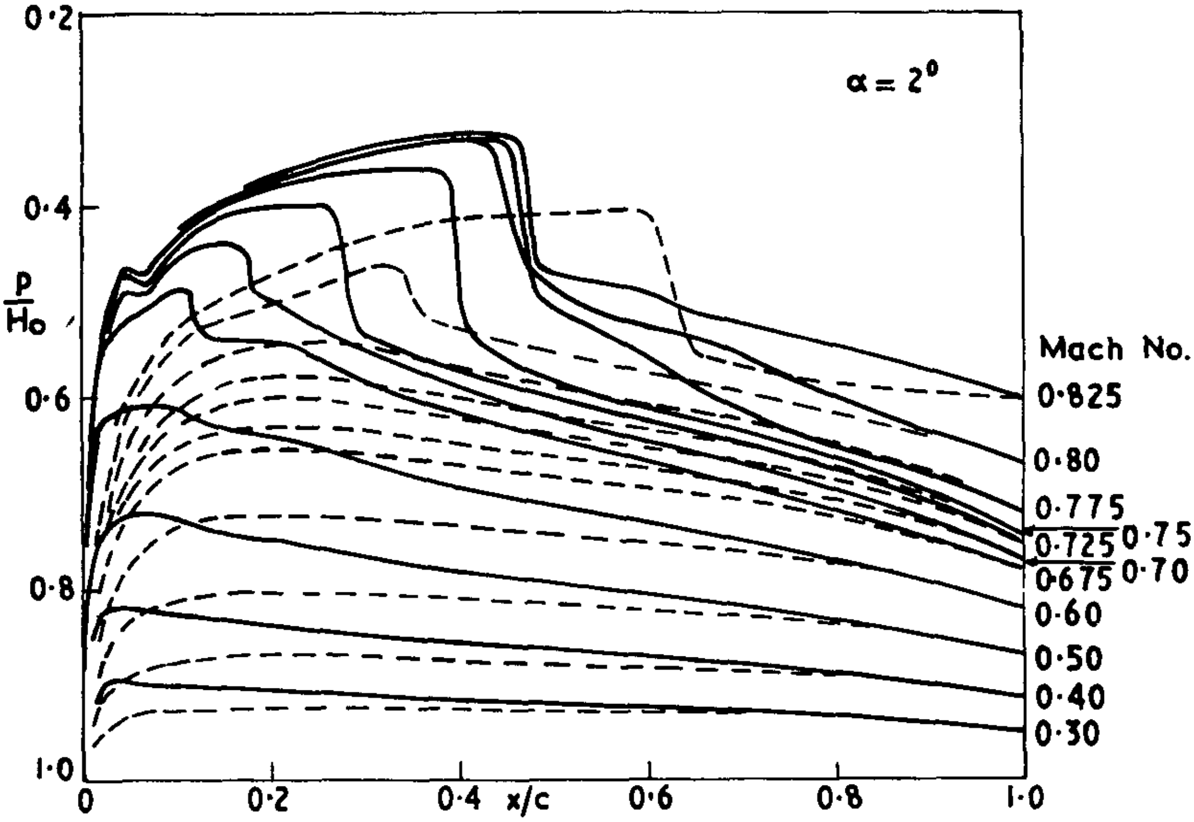

c NACA 0012 Pressure distributions, $\alpha = 2^0$

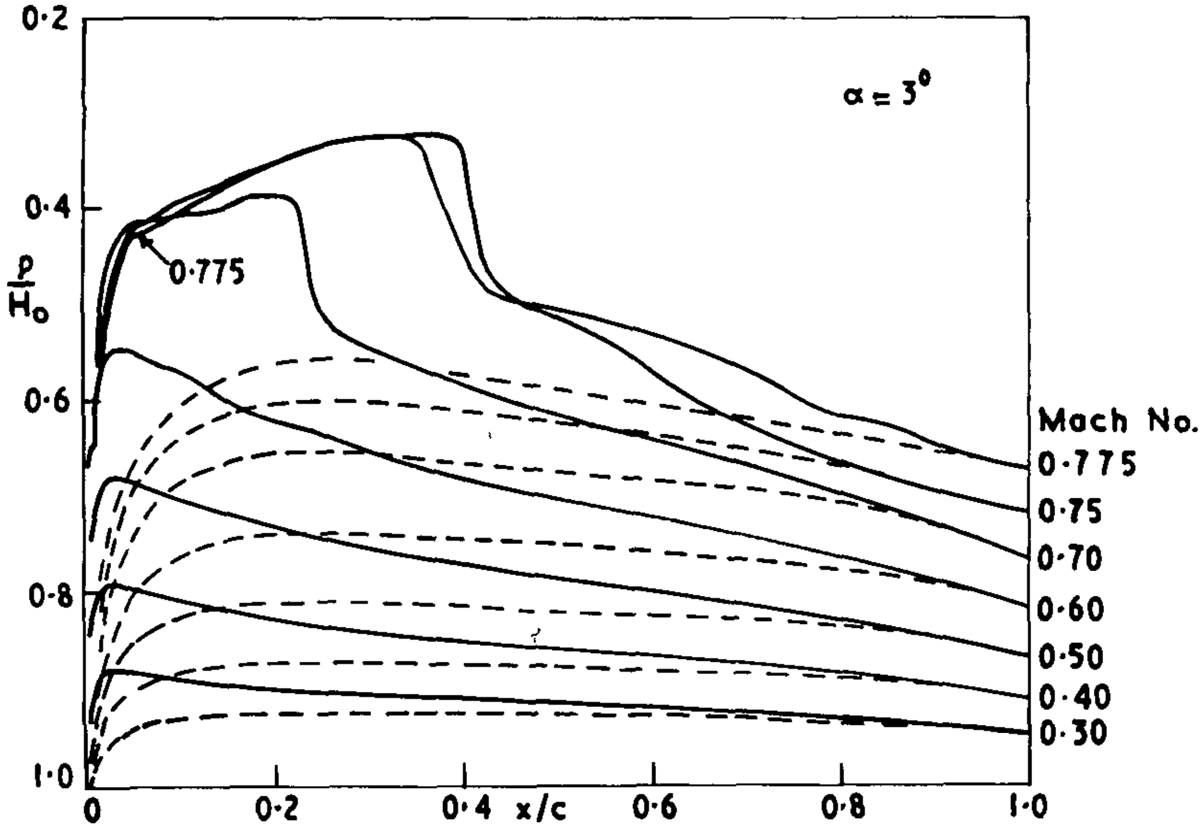

d NACA 0012 Pressure distributions, $\alpha = 3^0$

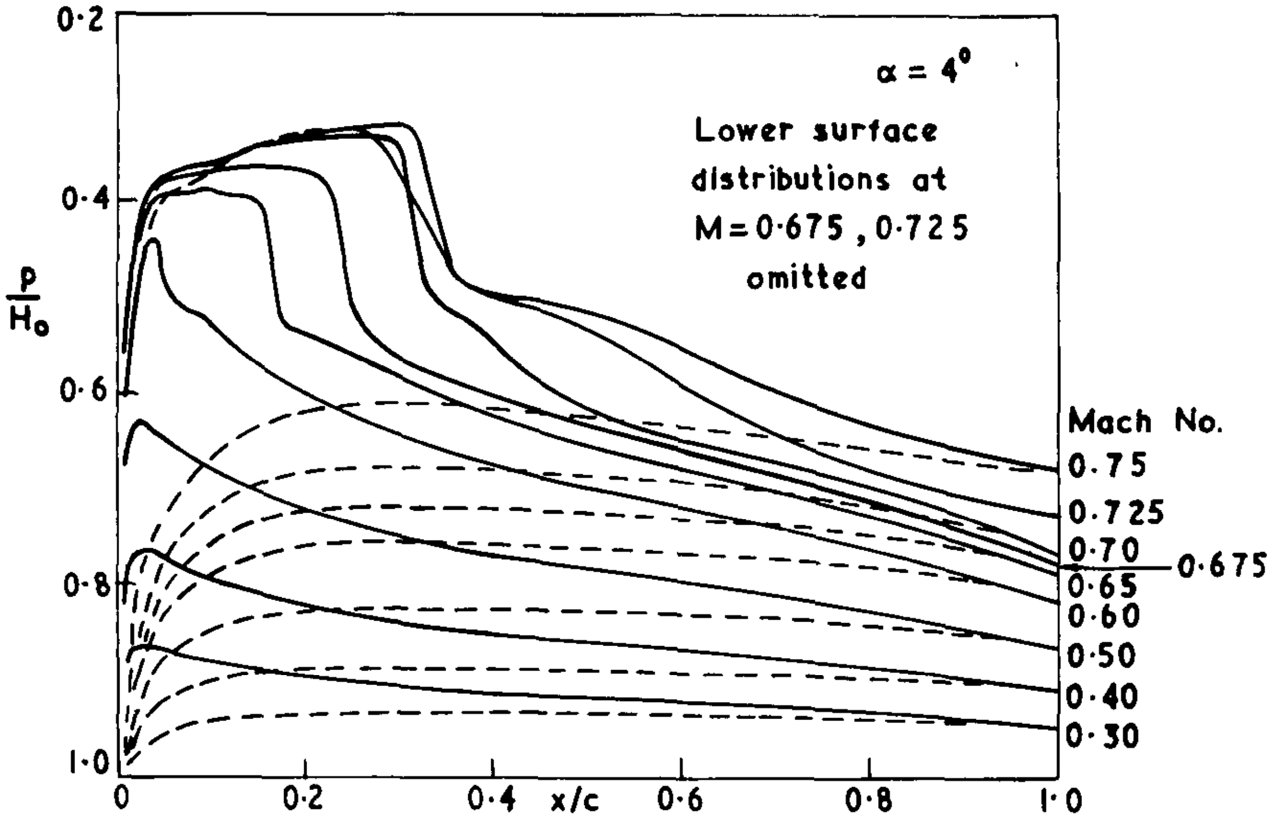

e NACA 0012 Pressure distributions, $\alpha = 4^{\circ}$

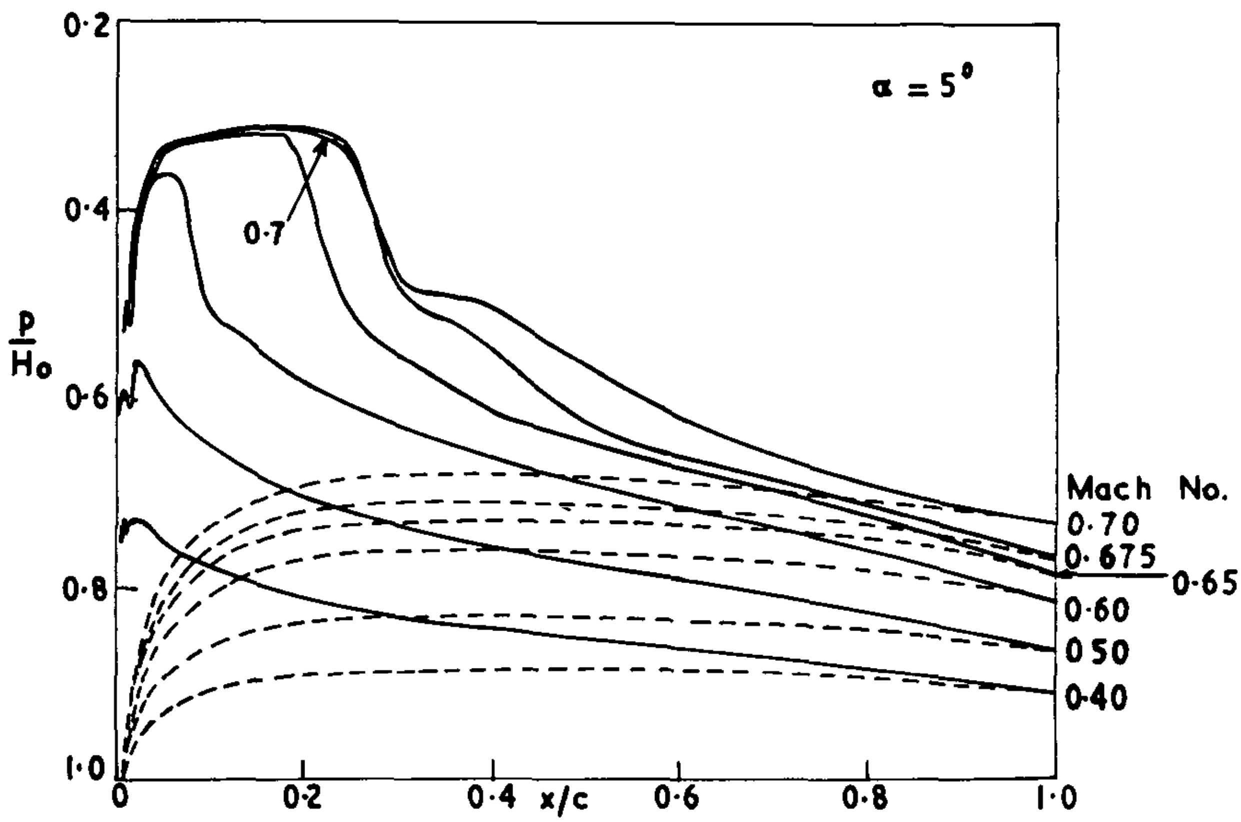

f NACA 0012 Pressure distributions, $\alpha = 5^{\circ}$

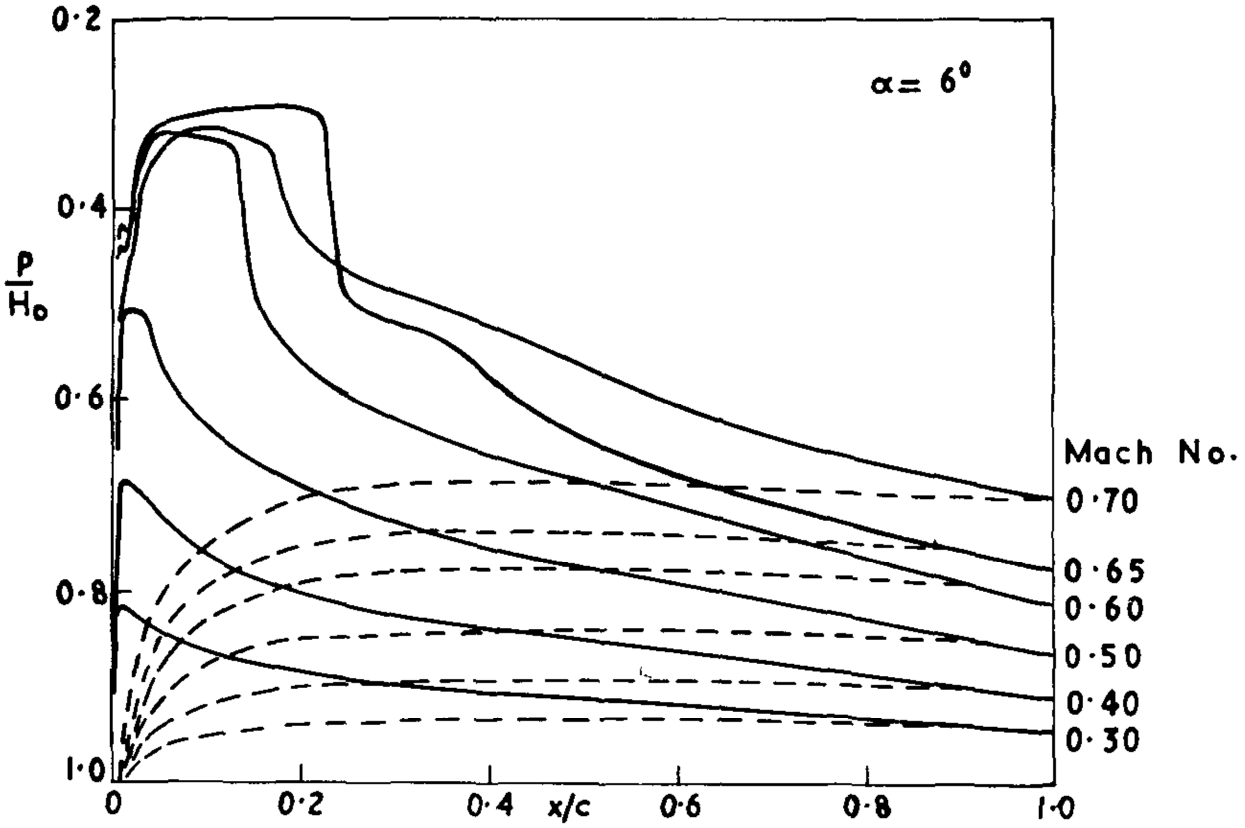

g NACA 0012 Pressure distributions, $\alpha = 6^{\circ}$

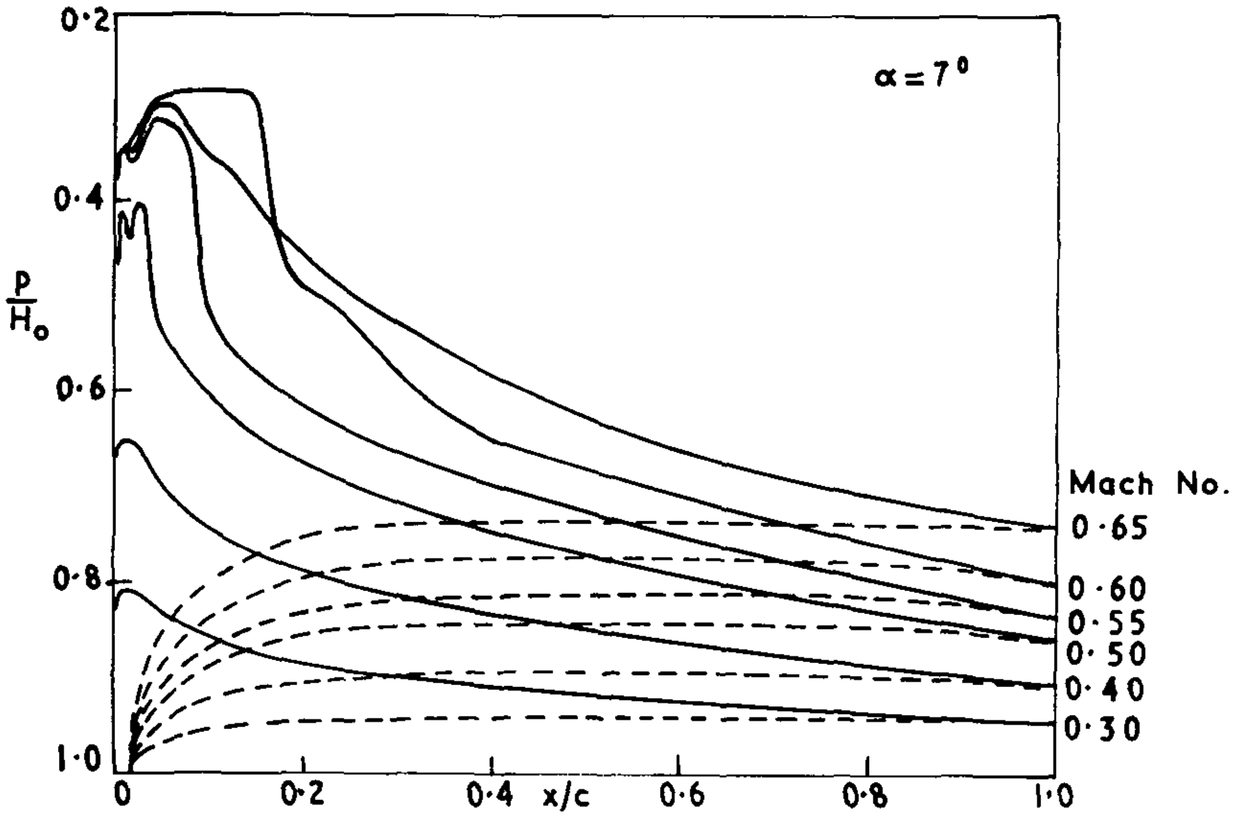

h NACA 0012 Pressure distributions, $\alpha = 7^{\circ}$

30657
FIG. 10 i & j

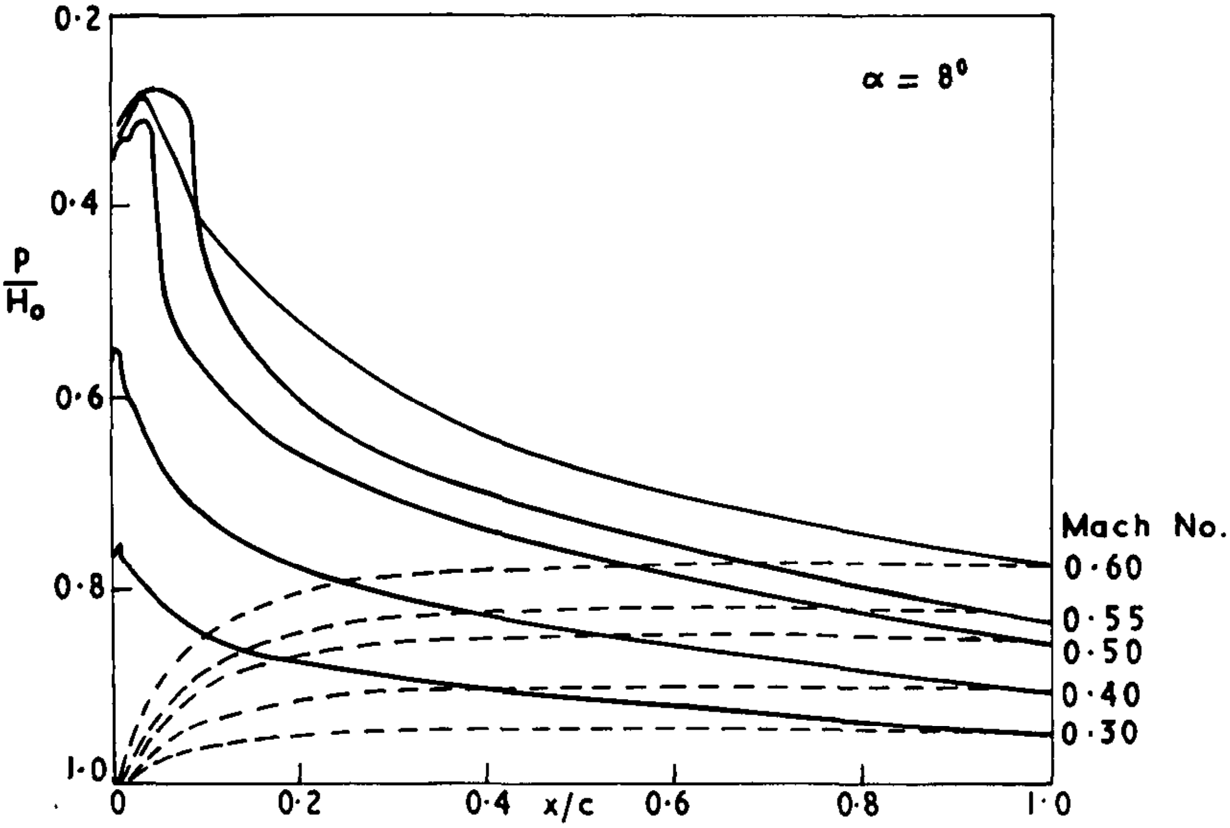

i NACA 0012 Pressure distributions, $\alpha = 8°$

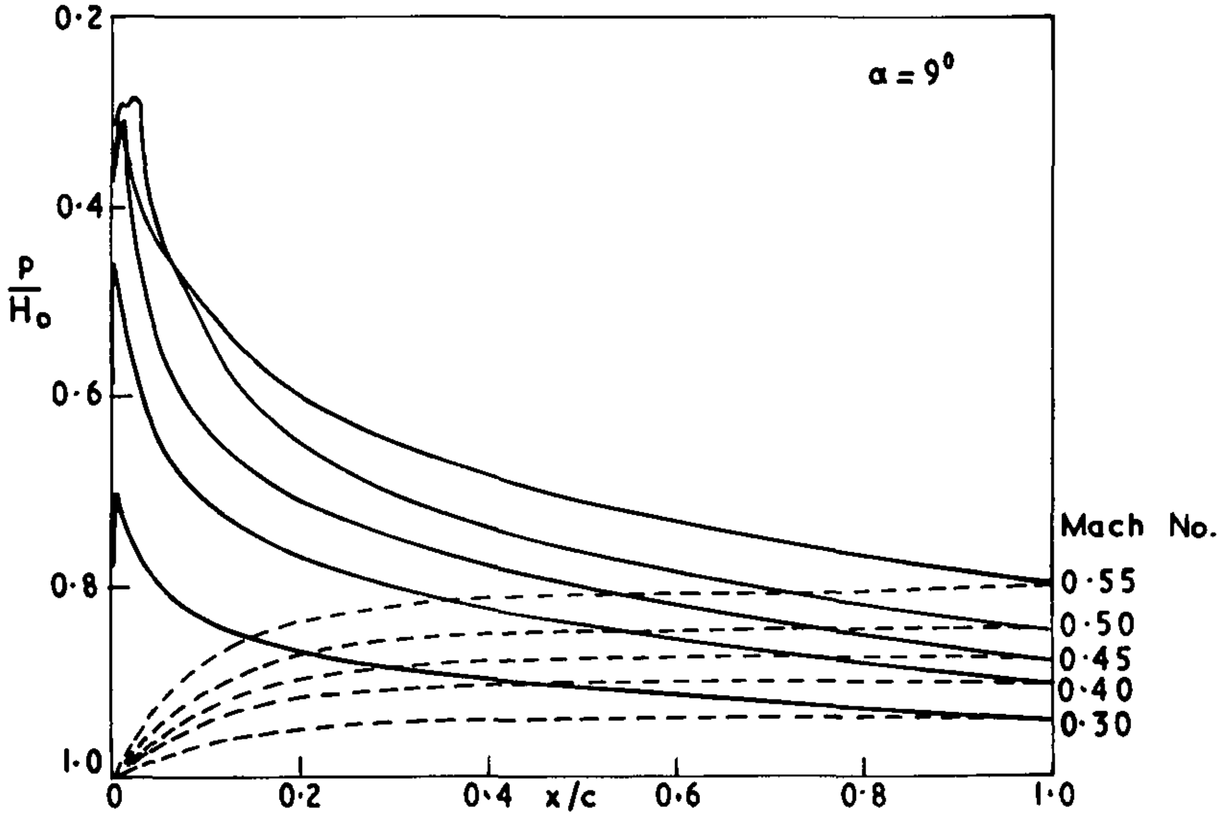

j NACA 0012 Pressure distributions, $\alpha = 9°$

FIG. 10 k & l

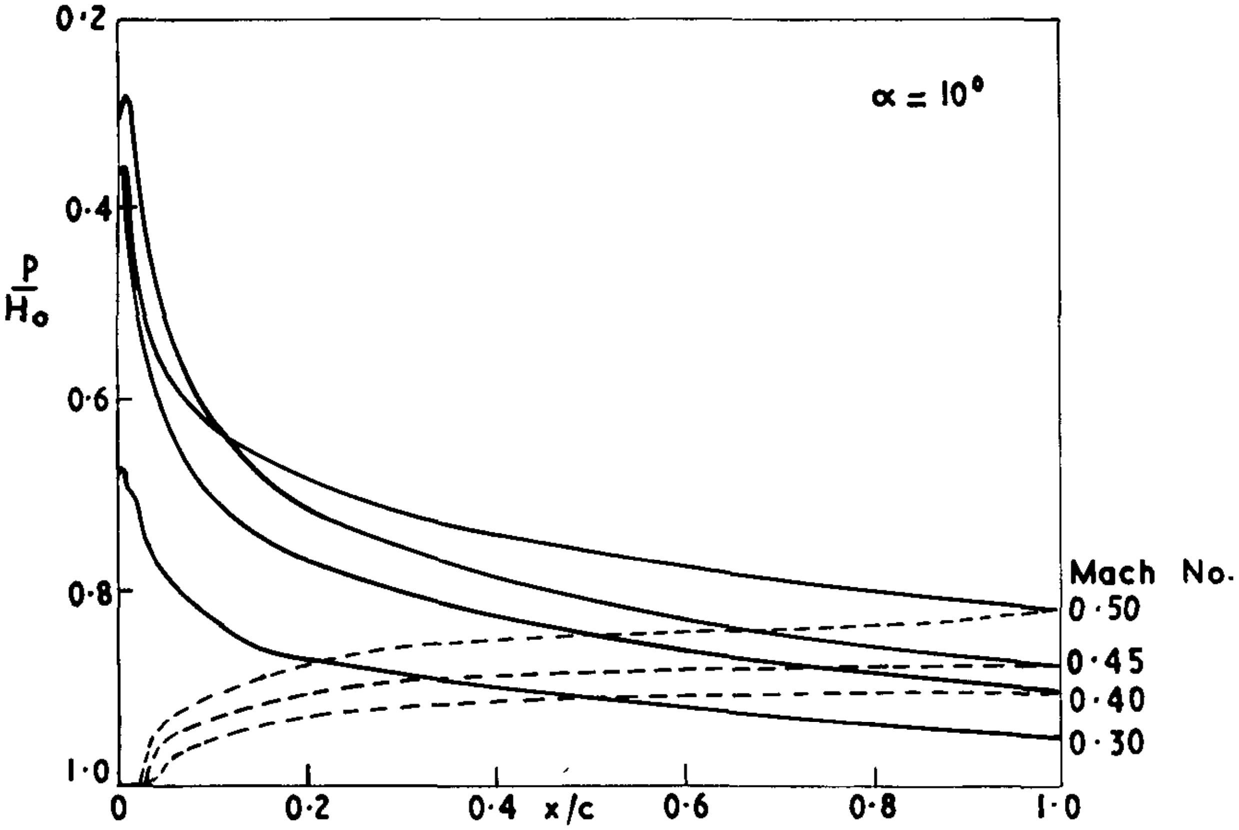

k NACA 0012 Pressure distributions, $\alpha = 10^\circ$

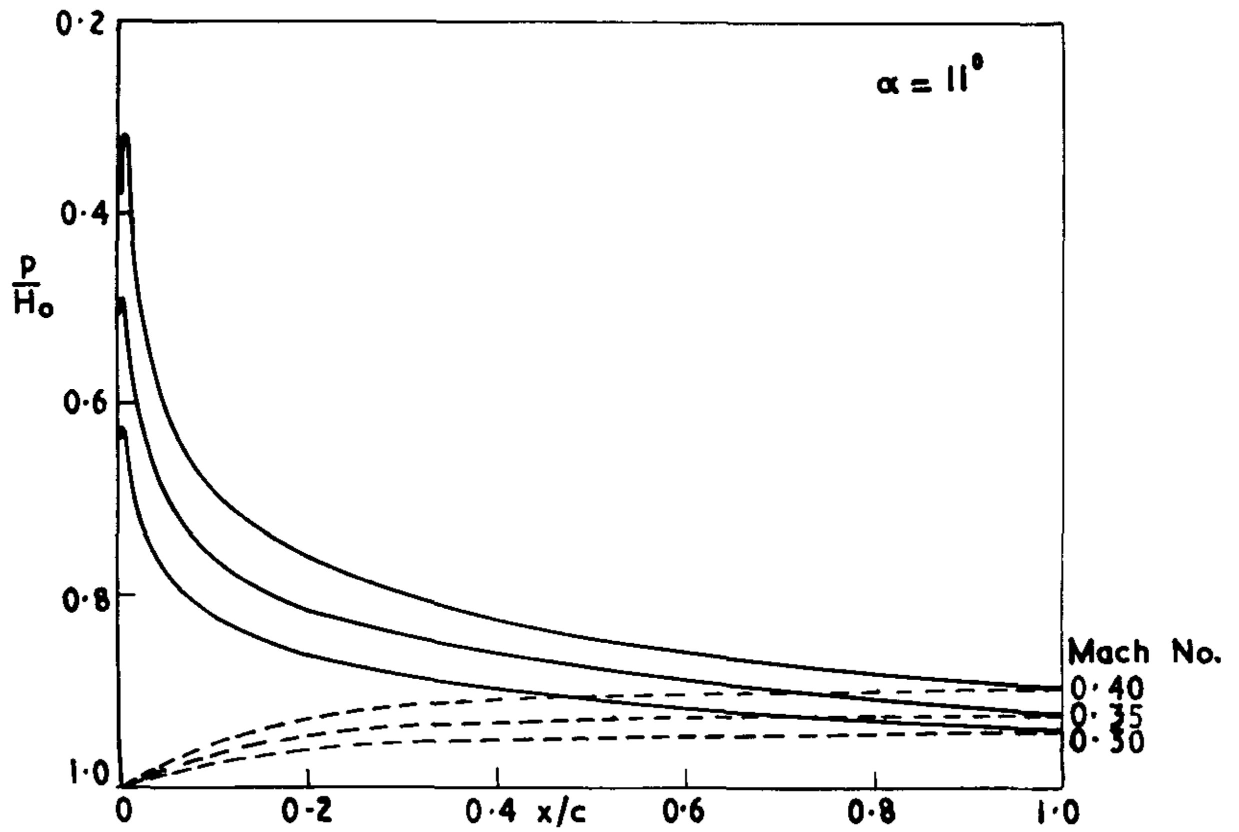

l NACA 0012 Pressure distributions, $\alpha = 11^\circ$

30 65 7

FIG. 10 m

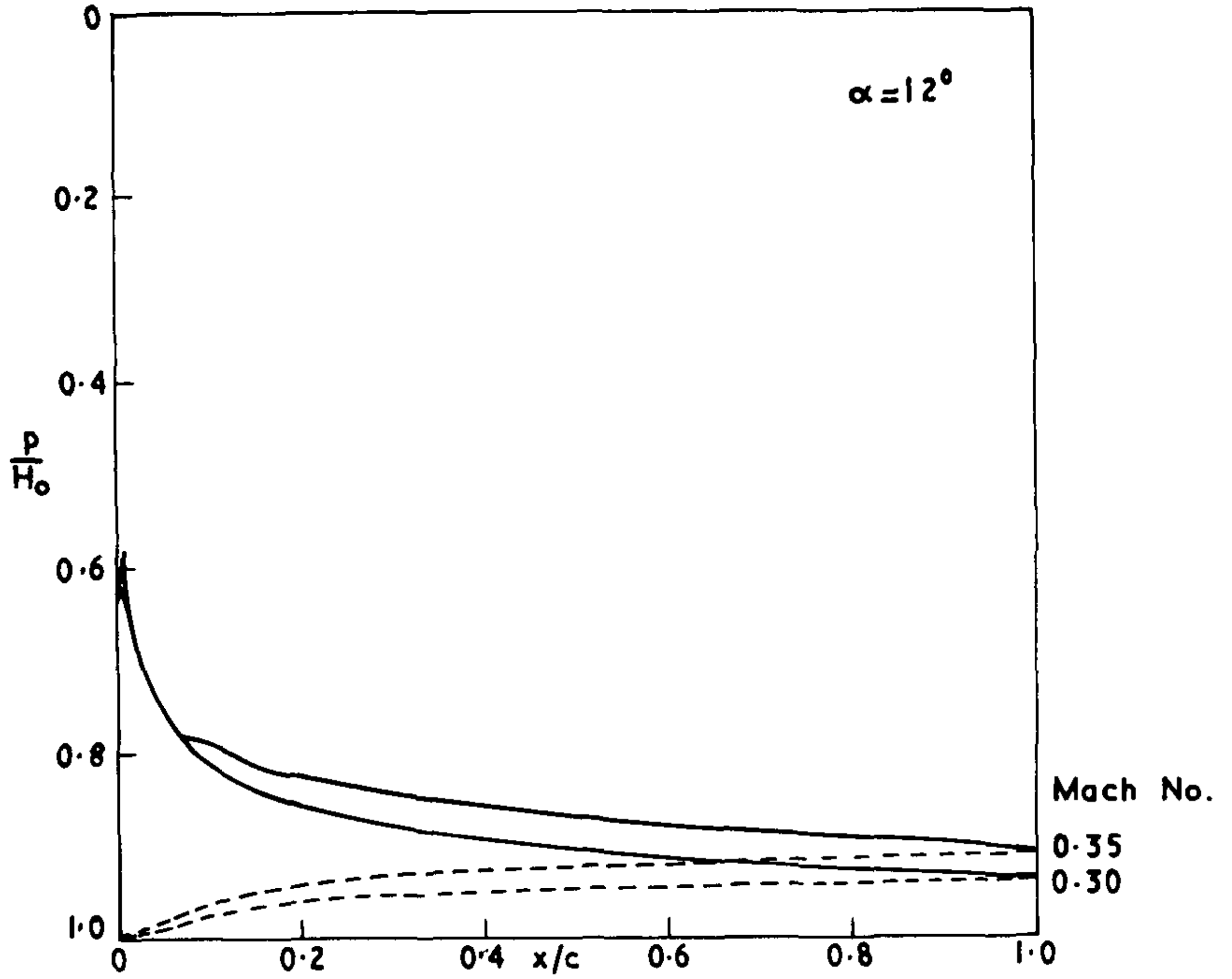

m NACA 0012 Pressure distributions, $\alpha = 12°$

30657
FIG.11

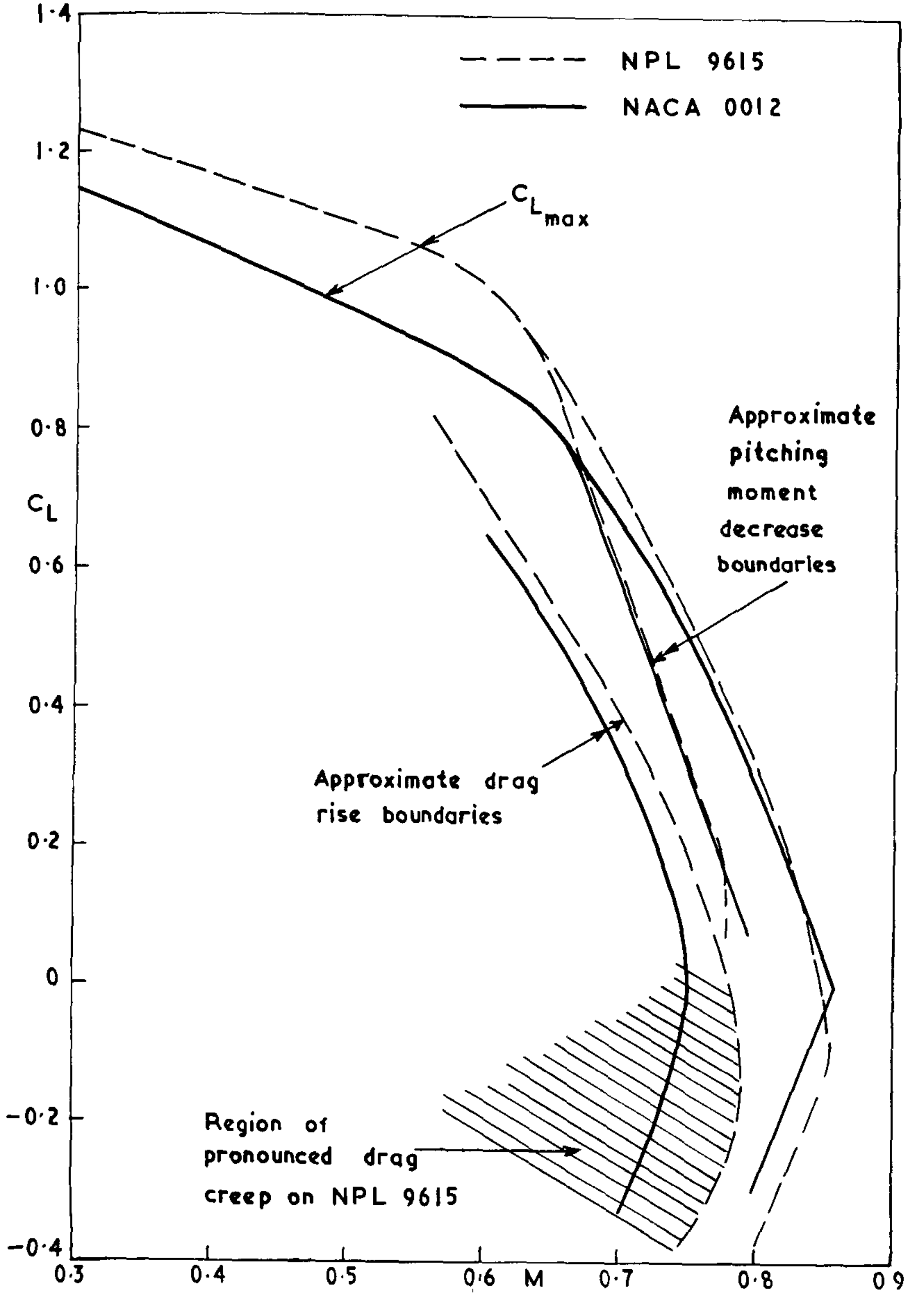

Comparison of limiting boundaries

30657
FIG. 12

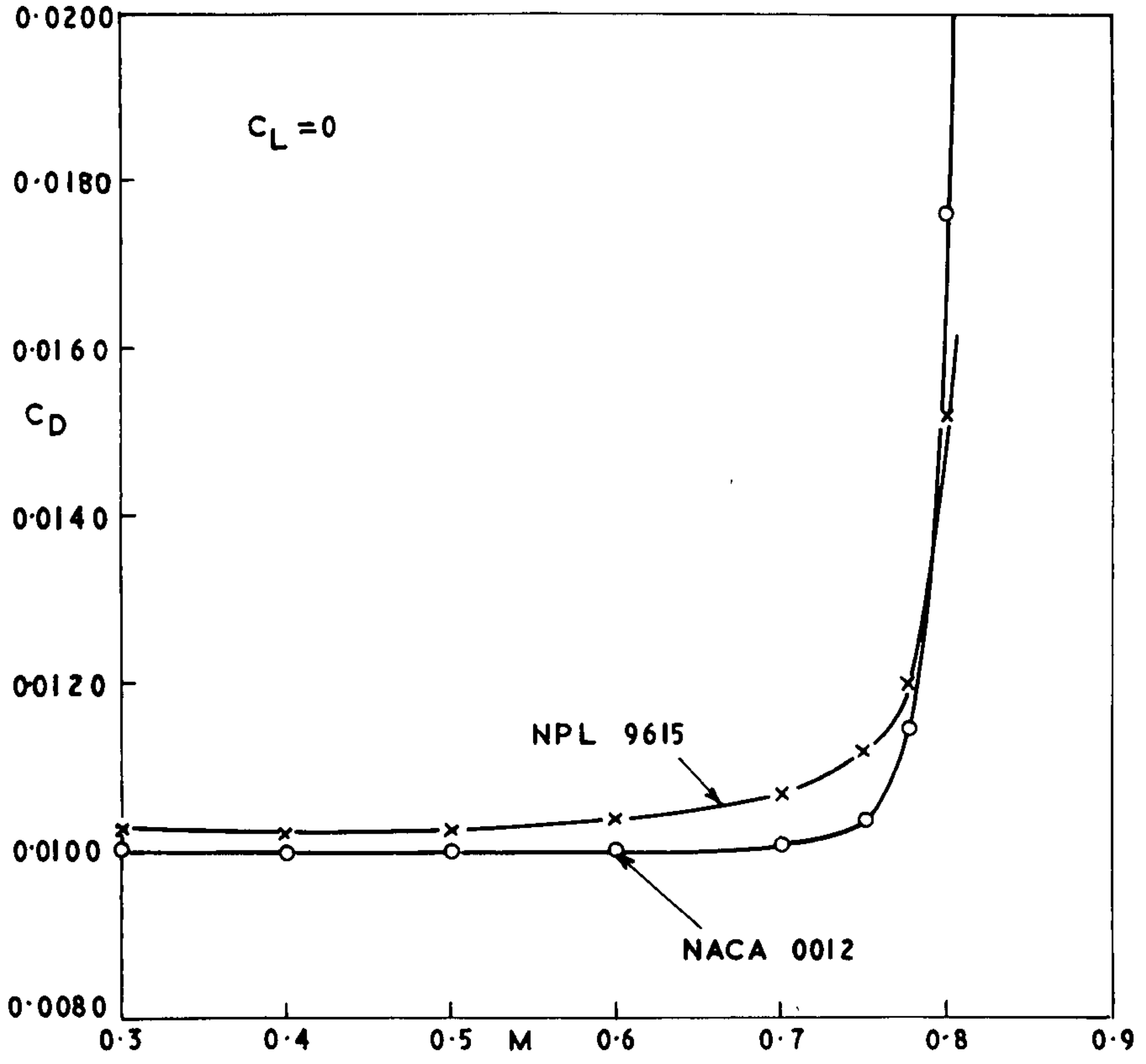

Comparison of variation of zero lift drag coefficient with Mach number

30657
FIG. 13.

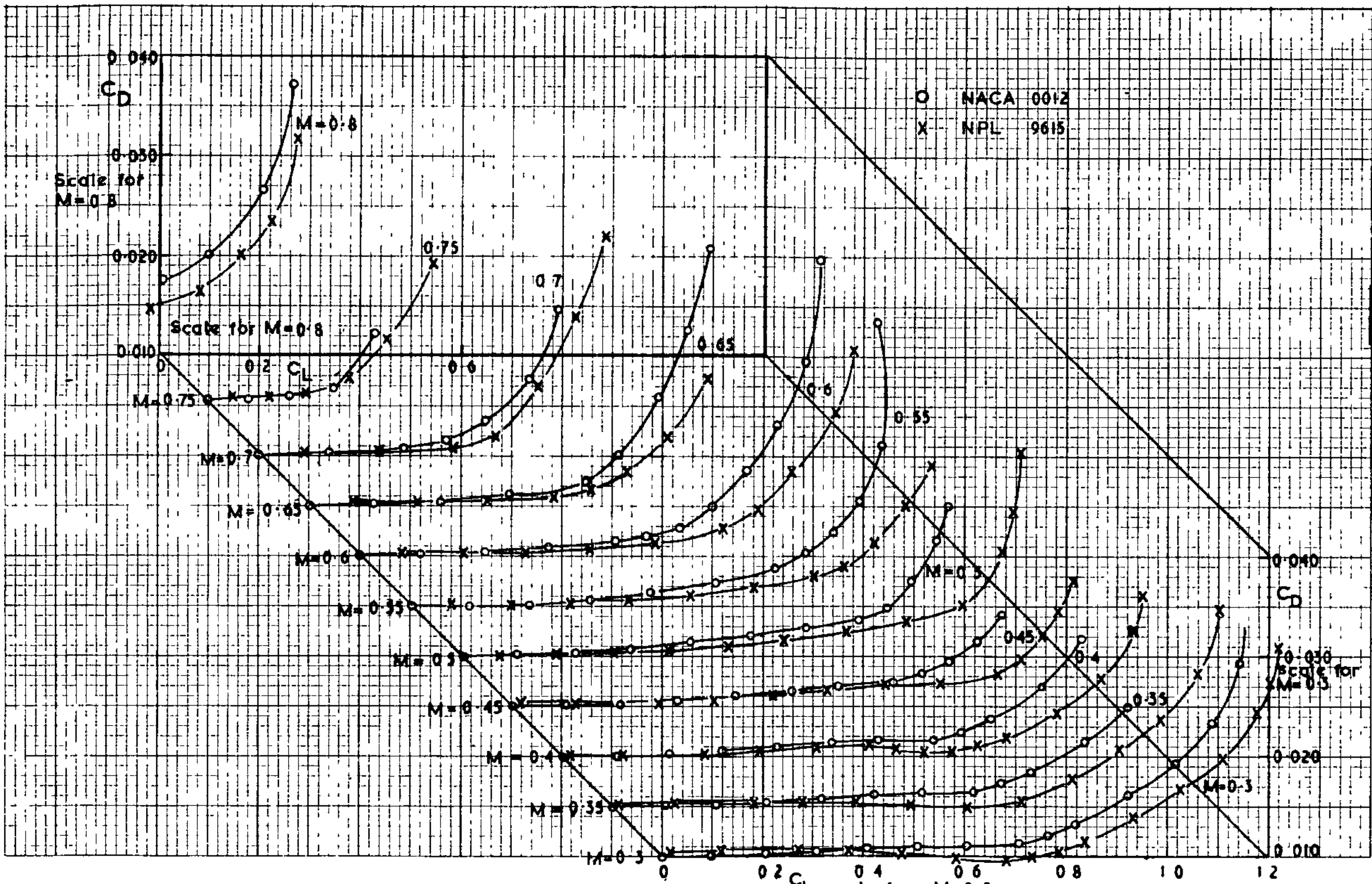

Comparison of drag polars

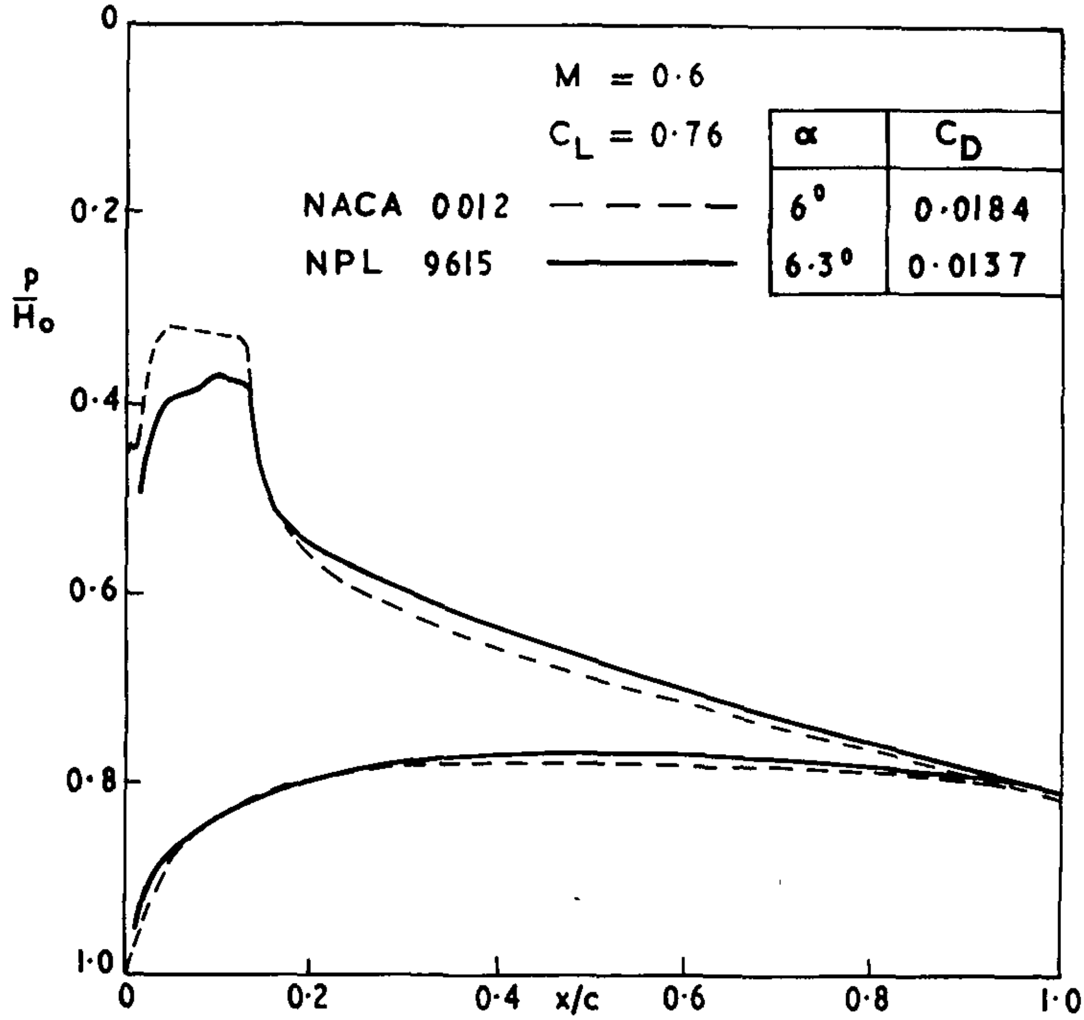

Comparison of pressure distributions at $C_L = 0{\cdot}76$
M = 0·6

30 657
FIG.15

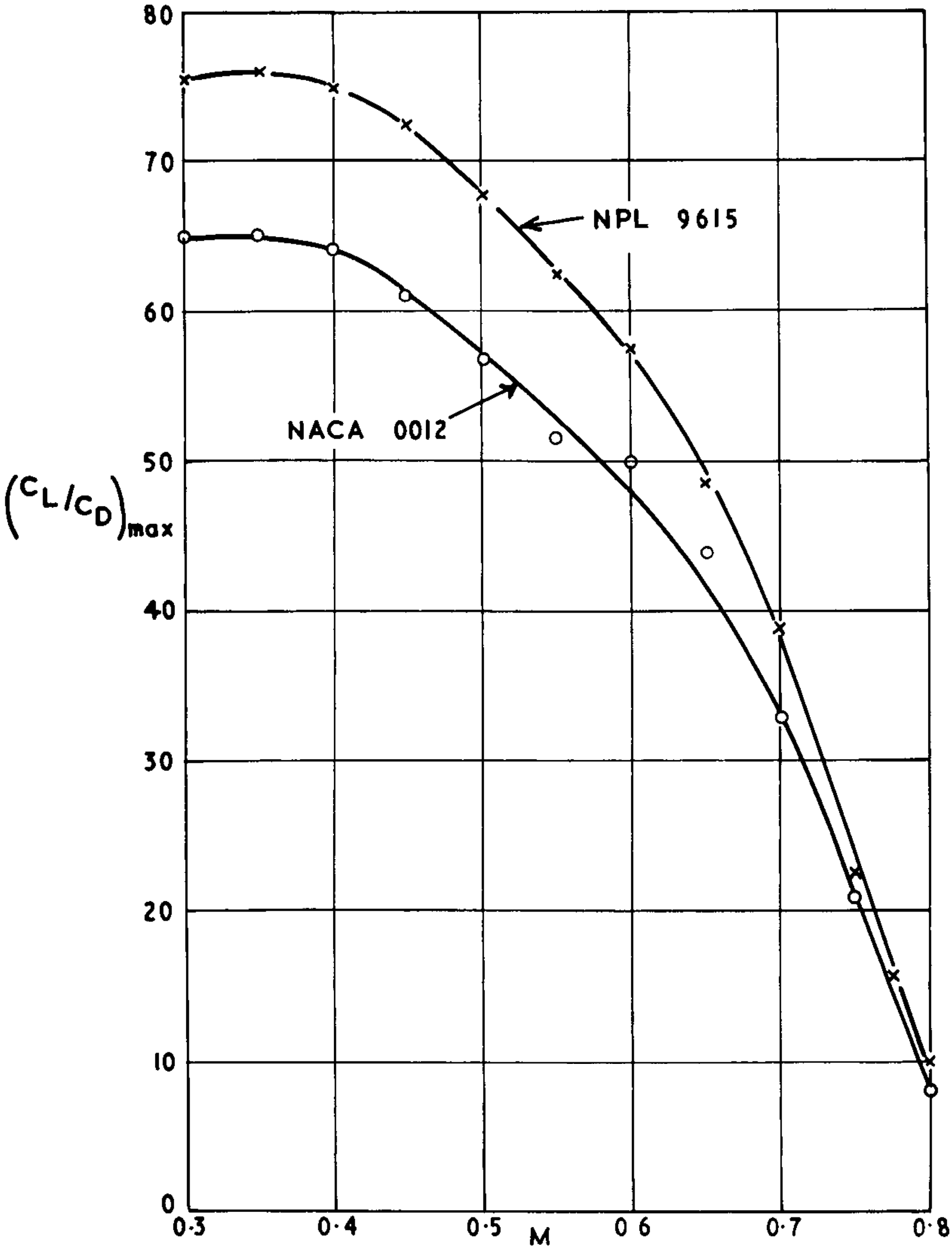

Comparison of variation at maximum lift / drag ratio with Mach number

30657
FIG. 16

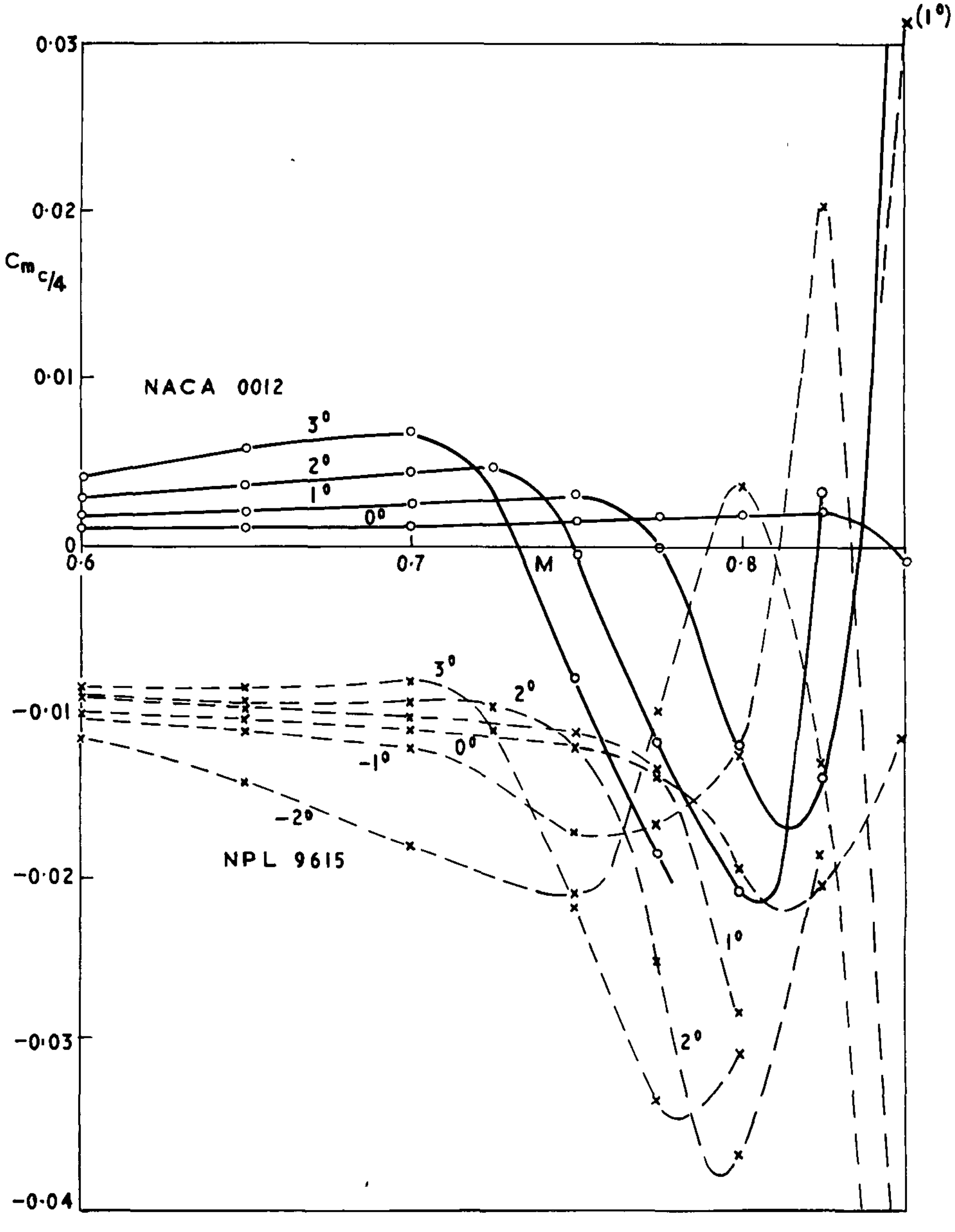

Comparison of the variation of the quarter-chord pitching moment with Mach number

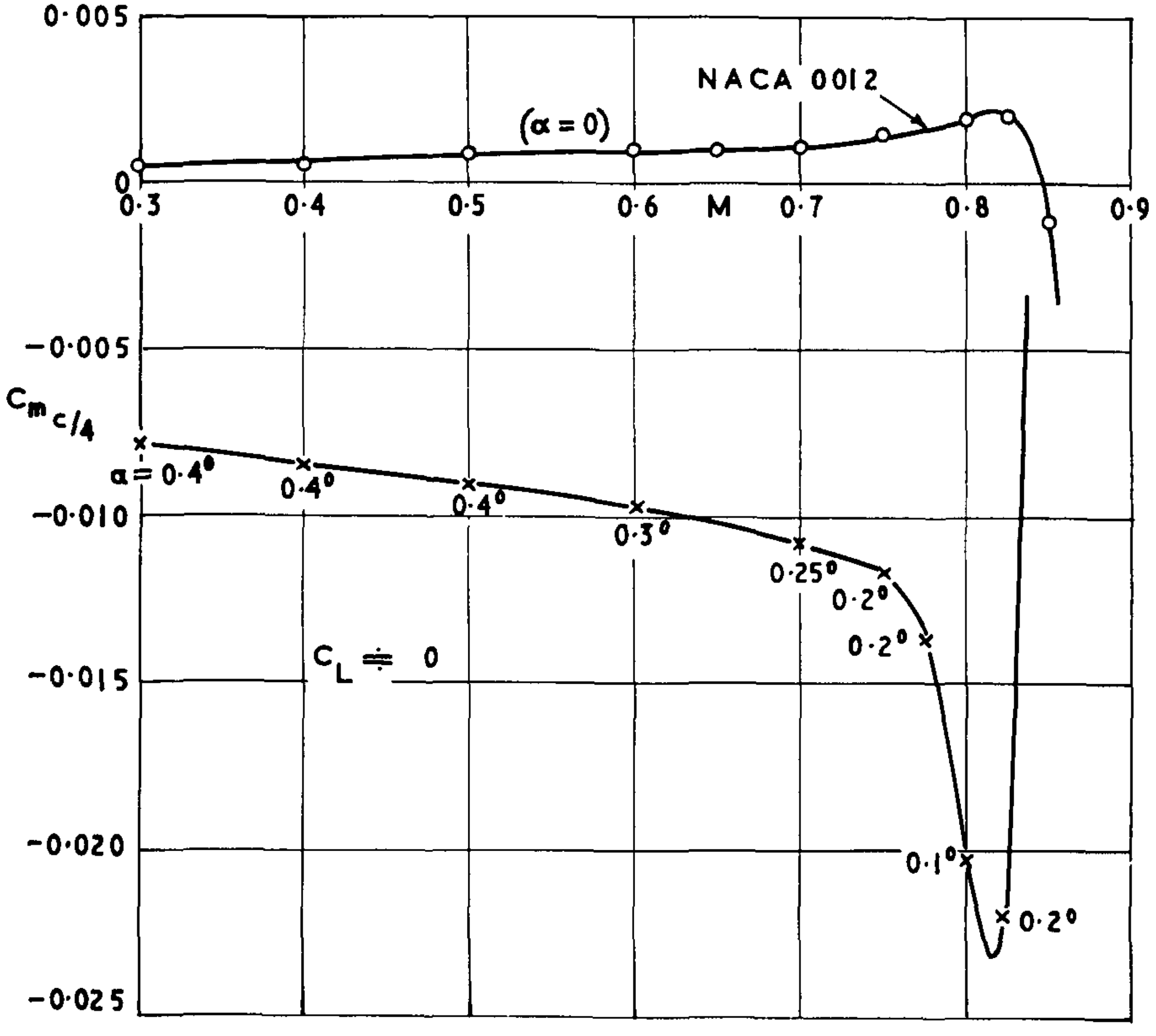

Comparison of variation of the zero-lift quarter-chord pitching moment coefficient with Mach number

R 69135/1/505716 K4 9/73 P

ARC CP No.1261
November, 1968
Gregory, N. and Wilby, P. G.

NPL 9615 AND NACA 0012 -
A COMPARISON OF AERODYNAMIC DATA

Ordinates, surface slopes and curvatures are listed for the two aerofoils together with a detailed tabulation of lift, drag and pitching moment data obtained at Mach numbers between 0.3 and 0.85 in the NPL 36 in. × 14 in. transonic tunnel. The aerodynamic characteristics and all the pressure distribution are plotted, with some comparisons.

ARC CP No.1261
November, 1968
Gregory, N. and Wilby, P. G.

NPL 9615 AND NACA 0012 -
A COMPARISON OF AERODYNAMIC DATA

Ordinates, surface slopes and curvatures are listed for the two aerofoils together with a detailed tabulation of lift, drag and pitching moment data obtained at Mach numbers between 0.3 and 0.85 in the NPL 36 in. × 14 in. transonic tunnel. The aerodynamic characteristics and all the pressure distribution are plotted, with some comparisons.

ARC CP No.1261
November, 1968
Gregory, N. and Wilby, P. G.

NPL 9615 AND NACA 0012 -
A COMPARISON OF AERODYNAMIC DATA

Ordinates, surface slopes and curvatures are listed for the two aerofoils together with a detailed tabulation of lift, drag and pitching moment data obtained at Mach numbers between 0.3 and 0.85 in the NPL 36 in. × 14 in. transonic tunnel. The aerodynamic characteristics and all the pressure distribution are plotted, with some comparisons.

DETACHABLE ABSTRACT CARDS

C.P. No. 1261

HER MAJESTY'S STATIONERY OFFICE

Government Bookshops

49 High Holborn, London WC1V 6HB
13a Castle Street, Edinburgh EH2 3AR
109 St Mary Street, Cardiff CF1 1JW
Brazennose Street, Manchester M60 8AS
50 Fairfax Street, Bristol BS1 3DE
258 Broad Street, Birmingham B1 2HE
80 Chichester Street, Belfast BT1 4JY

Government publications are also available through booksellers

C.P. No. 1261

ISBN 0 11 470819 3